WAGENINGEN UR
For quality of life

MSc thesis report

Evaluation of the Weather Research and Forecasting model for contrasting diurnal cycles in the Durance Vally complex terrain during the KASCADE field campaign

Author:

Peter Kalverla

Supervisors:

Gert-Jan Steeneveld (WUR)

Gert-Jan Duine (CEA)

Thierry Hedde (CEA)

October 24, 2014

DE LA RECHERCHE À L'INDUSTRIE

cea

CADARACHE

Evaluation of the Weather Research and Forecasting model for contrasting diurnal cycles in the Durance Vally complex terrain during the KASCADE field campaign

Peter Kalverla[1,2], Gert-Jan Duine[2,3], and Gert-Jan Steeneveld[1]

[1]Meteorology and Air Quality Section, Wageningen University, Wageningen, Netherlands

[2]Laboratoire de Modélisation des Transferts dans l'Environnement, CEA Cadarache, France

[3]Laboratoire d'Aèrologie, University of Toulouse, Toulouse, France

October 24, 2014

Abstract

For impact studies concerning the incidental release of effluents in industry, it is critical to understand and to be able to predict the meteorological conditions that govern the dispersion of these pollutants. In this respect, stable boundary layers form the most penalizing conditions, because mixing is limited and flow fields at different heights can become decoupled from one another. At the same time, the representation of stable boundary layers in atmospheric models remains challenging. In this study, the representation of the stable boundary layer in the Weather Research and Forecasting (WRF) model is evaluated for two contrasting nights at Cadarache, a nuclear research site embedded in the Durance valley in the southeast of France. With a mixture of mountains, hills and valleys, the region is best described as an area of moderate orographic complexity. Different land surface and planetary boundary layer (PBL) parameterizations are employed and sensitivity tests regarding land-surface-atmosphere coupling, soil moisture content and radiation parameterization are carried out. Measurements from two micro-meteorological towers, a sodar, and tethered balloon as gathered during the KASCADE campaign are used for model evaluation. The diurnal temperature range and PBL height are both highly underestimated by the model. The influence of the Durance valley on the wind pattern is recognized by the model, whereas orographic features on

smaller scale are missed. Even though the selected period is subject to substantial dry and warm air advection, the model performs well in representing this advection and the case remains suitable for evaluation of boundary-layer and land-surface parameterizations. We find marginal difference in model results for different PBL schemes. For the land-surface scheme, NOAH is found to give a slightly better representation than the 5-layer thermal diffusion scheme. Stronger surface coupling and lower soil moisture content both result in larger sensible heat fluxes, thicker boundary layers and a larger diurnal temperature range. However, such a large sensible heat flux is not supported by the observations. We conclude that the model is useful to obtain a general understanding of the meteorological processes that dominate the area, but for accurate dispersion estimates, a better representation of the vertical structure of the atmosphere is desirable.

1 Introduction

Stable boundary layers (SBLs) develop often during nights with clear skies and weak winds (Stull, 1988). The net negative radiation budget leads to cooling of the surface and consequently, a cold layer of air starts to form which extends upward as the cooling continues. In this layer, air density decreases with height and vertical motion (hence, mixing) is suppressed by buoyancy effects. Therefore, dispersion of pollutants is limited in SBLs (Zannetti, 1990).

Various processes act under stable conditions and the exact character of each SBL is the result of the delicate interplay between these processes (Mahrt, 2014; Steeneveld, 2014). First, there is the subtle balance between radiative cooling and the magnitude of the geostrophic wind (Van de Wiel et al., 2012). This determines whether turbulence is able to keep up with the cooling rate, or whether stratification increases to such an extent that turbulence is fully suppressed. In the latter case, a large temperature gradient builds up quickly in the lower atmosphere and at the same time, the flow field becomes laminar and the wind aloft may 'decouple' from that at the surface (Mahrt, 1999). In the decoupled layer, the wind tends to accelerate and form so-called low-level jets. If the extra shear produced by the accelerated wind becomes large enough to overcome the density stratification of the air, sudden episodes of intense mixing are observed (Kondo et al., 1978). Such bursts, referred to as intermittent turbulence, are found to contribute largely to the overall heat transport in the SBL (Poulos et al., 2002; Sun et al., 2012; Medeiros and Fitzjarrald, 2014). Another mechanism that can produce drag and lead to intermittency is gravity wave drag. Gravity waves can be induced by relatively small surface heterogeneities and their influence can be as large as, or larger than, the effect of shear-produced turbulent drag (Steeneveld et al.,

Mountains also exhibit important effects on the stability and the flow. On slopes, the cooling near-surface air starts to sink to the valley floors and so-called 'cold pools' form in the valleys (Price et al., 2011). The warmer air is lifted in the middle of the valley and the result is a strong temperature inversion at the interface between the cold pool and the warmer air aloft. This inversion acts like a lid on top of the valley, preventing vertical mixing and decoupling the flow aloft. Down-valley flows are often observed, draining the cold, dense air like a river (Whiteman, 2000). The influence of orography on the wind field is not limited to katabatic effects, such as the sinking of cold, dense air to the valley floors. Other processes that occur are e.g. wind channeling by the valley walls or distinct valley flows due to local pressure perturbations (Whiteman and Doran, 1993; Carrera et al., 2009).

Model performance for the SBL has been studied within the context of the GABLS model intercomparison studies. Holtslag et al. (2013) summarize the results and conclude that state-of-the-art models can simulate moderately-stable boundary layers over flat, homogeneous terrain, but very stable boundary layers over heterogeneous terrain are still not well represented. Correct atmosphere-land-surface coupling is found to be essential for a good representation of the diurnal cycle of the boundary layer. Bosveld et al. (2014) shows that the representation of the morning and evening transitions, i.e. onset and decay of turbulent mixing due to sunrise and sunset, respectively, can deviate by 2 hours for a relatively simple case. Another important process in SBLs, is radiative flux divergence (Brutsaert, 1972; Manins and Sawford, 1979; Manins, 1992). This process helps to overcome the temperature gradient as imposed by the surface cooling. Steeneveld et al. (2010) found that the MM5 mesoscale model underestimates this term by a factor 10. A previous study dealing with SBLs and complex terrain (Cuxart et al., 2007) used a very high vertical resolution to reach satisfactory results. However, this requires a lot of computational power.

It is clear that a good understanding of the SBL is critical for dispersion studies, because mixing of pollutants is very limited under these conditions. The current study focuses on the dispersion of effluents in the surroundings of Cadarache, one of the research facilities of the French Centre d'Energie Atomique (CEA). Located in the southeast of France, Cadarache is situated in a small valley that merges with the larger Durance valley. This region of France, the Provence, is known for its clear skies, is generally very dry and is characterized by a large diurnal temperature range. All these conditions, along with the mountainous topography, favor the formation of stable stratification and give rise to the complex behavior of the atmosphere as described above. As such, it is a very challenging terrain.

In the winter of 2013 the extensive measurement campaign KASCADE (KAtabatic winds and Stability over CAdarache for Dispersion of Effluents) has been carried out in the study area (Duine et al., 2014a,b). Exhaustive measurements (section 2.1) were performed to characterize the (stable) boundary

layers in the Cadarache valley, and to obtain data for model input and validation. The campaign resulted in 23 successful intensive observational periods (IOPs) and a unique dataset that is ideally suited to study the challenging conditions that characterize our case.

The goal of the current study is to assess and possibly improve the capability of the Weather Research and Forecasting (WRF) model (Skamarock and Klemp, 2008) to predict the meteorological conditions that are important for the dispersion of pollutants in the study area: wind, stability and mixing. A good model simulation would complement the KASCADE measurements and help us understand important phenomena like the Durance valley wind (a typical valley wind that is often observed in the area), and can be used as input for dispersion studies.

We evaluate different planetary boundary layer (PBL) and land-surface parameterizations and perform sensitivity analyses with respect to the radiation parameterization and soil moisture content. We pay much attention to surface-atmosphere coupling and the representation of the diurnal temperature range (DTR). We formulate the following research questions: Is WRF able to represent the large DTR that is characteristic for the area? Are the stratified nocturnal temperature and moisture profiles realistically represented? Does the model correctly simulate the wind speed and direction during the night? Is the evening transition well-captured?

In the following sections, we will discuss the study area and explain our domain configuration and IOP selection (sections 2.1, 2.3). In section 3 we explain the different model configurations we tested. A first evaluation of the results is given in section 4. Then, we discuss the results of our sensitivity analyses regarding surface coupling, radiation schemes and soil moisture (sections 4.2). Finally, we present the modeling results in a comprehensive way that complements the KASCADE measurements, and we discuss the most important shortcomings of the model (section 4.3). We summarize our findings in section 6.

2 Study area and case selection

We will first present our domain configuration and study area . Then we will briefly summarize the measurements that where taken during the KASCADE campaign. At the end of this section we explain our IOP selection and present a first characterization based on the KASCADE data.

2.1 Study area and domain configuration

The study area is located in the Provence in the southeast of France. The elevation of Cadarache is 250-300 m above sea level; the landscape is dominated by hills and moderately high mountain ridges of 1000-1250 m (Saint Victoire, Luberon). The Plateau de Valensole, which has an average elevation of 500

m and a slight southwest-facing slope, separates the area around Cadarache from the Southern Alps. The Mediterranean sea is found at 80 km from Cadarache. Soils in the area are rich in limestone and typical vegetation types are herbaceous shrubs, pine trees and evergreen oaks (Ganteaume et al., 2009). Due to the frequent occurrence of the mistral wind and the surrounding mountains, the skies are often very clear and sunshine is abundant throughout the year (> 2500 hours, Wrathall, 1985). Summers are usually warm and dry, while winters are cold due to the vicinity of the Alps.

As mentioned above, the mistral occurs frequently in the area. This is a strong northwesterly wind that can sometimes reach speeds of 30 ms^{-1}. Another wind that is often observed is a weaker north-easterly flow which we labeled as the Durance valley wind. It occurs frequently at night, especially under stable conditions. It flows along the middle Durance valley, with wind speeds of ~5 ms^{-1}. The mechanism governing this wind is not clear, but some hypotheses invoke a weak valley-flow due to the local slope, a drainage outflow from the Alps, channeling of the wind aloft or a combination of these.

We use four nested domains to encompass all important orographic features and meteorological phenomena in a large area around Cadarache(figure 1A). The outer grid covers the large mountain areas and the influence of the Atlantic Ocean and the Mediterranean Sea. The second domain covers the Alps (partly), Pyrenees and the Massif Central and should solve the Mistral wind and the common low pressure area between Corsica and the continent. The third domain should solve mesoscale phenomena like the sea breeze and deflected mistral winds. Finally, the fourth domain represents the Durance valley area with the highest surrounding mountains.

Figure 1B shows the extent of the fourth domain, while figure C highlights the most important characteristics of the study area. The dominating feature is the middle Durance valley, which has a length of around 50 km, with a depth of approximately 200 m. Its average width is 5 km and it has an average slope angle of 0.2°. To the southwest, the valley narrows to 200 m near the Clue De Mirabeau (CdM). Cadarache is situated in a small side valley near the CdM. This valley has a width of 1–2 km and a length of 6 km.

One of the difficulties in modelling over complex terrain is that slopes are often smoothed in relatively course scale meteorological models such as WRF (Jiménez and Dudhia, 2012). We run WRF on a horizontal resolution of 1 km in the inner domain, which is among the highest resolutions found in WRF modelling studies. Increasing the resolution beyond this point results in high computational costs and physical limitations of the model (Arnold et al., 2014). Given this 1 km resolution, we expect the model to resolve processes on the scale of the Durance valley. The Cadarache valley itself is too small to be represented on this scale. Figure 1D shows how WRF 'sees' the orography. As compared to figure 1B, many small scale features are smoothed, but the Durance valley is still quite well represented, as well as the CdM. Indeed, the Cadarache valley is smoothed and barely recognizable. We use 35 vertical levels,

the first of which is found at approximately 25 m above the surface.

2.2 The KASCADE dataset

The dataset from the KASCADE campaign comprises continuous measurements from three sites, as well as additional measurements obtained during 23 intensive observational periods (IOPs). First of all, a high mast is routinely operated by CEA Cadarache, which measures wind and temperature at 110 meter. Since the top of this mast is higher than the depth of the Cadarache valley, it measures the flow in the larger Durance valley. Further, a meteorological station is situated at the northernmost edge of the Cadarache centre that measures 2-m temperature, humidity and pressure and 10-m wind speed. For the KASCADE campaign, a SODAR was placed near the meteorological station, measuring wind speed and direction up to ~500 m. In the heart of the Cadarache valley, a 30-meter flux tower was installed and equipped with three sonic anemometers (2, 10 and 30 m) yielding 30-minute averaged eddy-correlation fluxes for heat (H), momentum (u^*) and moisture (LvE, only at 30 m), and two radiometers (1.2 and 20 m). During IOPs, radiosoundings were launched at 12, 18, 00 (only in the last week) and 06 UTC and tethered balloon measurements were carried out, profiling the lower 0-300 m of the atmosphere to obtain nearly continuous profiles of wind speed and direction, temperature, humidity and pressure.

Because the 30 m mast, tethered balloon and radiosonde measurements where all carried out in the heart of the Cadarache valley, they are likely to have measured some influences of the Cadarache valley that the model cannot distinguish. For example, a katabatic wind was often observed, changing the wind speed, direction and temperature and humidity profiles inside the valley. This is important to keep in mind while evaluating the model with these observations.

2.3 IOP selection and characterization

Based on a nearly impeccable radiation balance and contrasting wind fields, we have selected the period between 18 Feb 2013 12:00 UTC - 20 Feb 2013 12:00 UTC for our model evaluation. This 48 hours period covers exactly two IOPs, so that we have abundant measurements to validate our model output. The first 6 hours are considered as model spin-up, so we evaluate the results from 18 Feb 18:00 UTC.

Figure 2 shows that synoptic pressure gradient over the study area is small during the selected period. At the beginning of the simulation, a high pressure area is situated over a large part of Europe, reaching from the United Kingdom to the Black Sea. Together with some cyclonic rotation over the Atlantic, this results in a weak southeasterly flow over the study area. After 24 hours, the high pressure area has disintegrated and lows over Poland and Greece induce a northeasterly flow over France. Because the overall pressure gradient is still low, we expect that processes on the synoptic scale are of minor

6

importance for the evolution of the boundary layer at the study site. These are perfect circumstances for strong stable boundary-layer development.

Before we investigate the model performance, we study the behaviour of the PBL by examining the KASCADE data. Figure 3A and -B show that, indeed, the wind pattern is fairly different between the two IOPs. There is a south/southeasterly wind at the beginning of IOP15 with wind speeds of 4-6 ms^{-1} in the lower 500 m. Around 21:00 UTC, wind speed decreases and the wind direction turns to northeast, starting from the surface. This the typical Durance valley wind that we described above. On the second day, the wind is much stronger, up to 10 ms^{-1}, and from the west/northwest. This seems to be a rather weak manifestation of the mistral. After sunset, wind speeds drop and the wind turns to the north and slightly northeast, but this effect much less pronounced than in IOP15. Note that the color scale is not cyclic, so the strong gradient around the north component is somewhat misleading.

In figures 3C and -D reveal that there is advection of warm and dry air. We deduce the PBL height from the strong gradients of potential temperature and mixing ratio. It is substantially higher on 18 February (∼1900 m) than on the 19th (∼1400 m). Such thick PBLs even in winter are characteristic for this area. The figure also depicts the development of the SBL and illustrates the large DTR. At 06:00 UTC (both nights), the surface potential temperature drops to 270 K, while it reaches a maximum of 286 K around noon. We find drying in the lowest part of the PBL during the night, pointing to formation of dew. Drying continues until noon due to the entrainment of dry air during the PBL growth in the morning. Between noon and sunset, the humidity of the PBL increases due to evapotranspiration.

To identify the source of the warm and extremely dry air that is advected, we employed the HYSPLIT backward trajectory analysis of the NOAA Air resources laboratory (Draxler and Rolph, 2003). The results are shown in figure 4. If we look at the figure for 19 February, we see that the air at 2000 meters has been advected over the Alps and we infer that a foehn-effect has taken place, i.e. the air has lost its moisture due to precipitation on the windward slopes and subsequently warmed due to orography-induced subsidence at the west end of the Alps. This explains why we find very low values of specific humidity in figure 3C. What we can also learn from the figure is that the source of the advected air is very different for the different altitudes that we plotted. This is an implication of the choice for a weak synoptic situation. Apparently, the absence of a strong forcing allows the formation of several distinct flows on different scales. This affirms the need to study these processes in order to make correct estimates for dispersion of pollutants.

3 Model configuration

In this section we will explain our model configuration. We will start with the general settings that we used for all runs. Then, we will explain the different land-surface and PBL schemes that we used. Each PBL scheme is combined with a surface layer scheme that computes the turbulent transport near the surface and as such it provides the lower boundary conditions for the PBL parameterization. We will elaborate more on the surface-layer parameterization in section 4.2.1.

3.1 Default settings

The default settings are listed in table 1. For the land use we choose for the Corine Land Cover (Büttner et al., 2002) because it is more recent (2006) than the commonly applied USGS landuse (1992) and has a higher resolution (250 m versus 900 m). An evaluation of the Corine land cover can be found in De Meij and Vinuesa (2014). They find improvements of wind, temperature and precipitation forecast on high resolution simulations (1 km). We use the European Centre for Medium-Range Weather Forecasts (ECMWF) operational analysis input data with a spatial resolution of 0.25°on 20 pressure levels. This horizontal resolution corresponds with the resolution of our outer domain. Table 2 shows the different parameterizations that we use for the PBL and the land-surface.

3.2 Land surface parameterization

The land-surface scheme plays a very important role for the partitioning of the available energy at the surface. It computes the sensible, latent and soil heat fluxes and also skin and soil temperatures. Surface characteristics like albedo, emissivity, soil moisture and conductivity are either read from climatological tables, or computed interactively, dependent on the complexity of the model. We use two schemes of contrasting complexity for our study. The MM5 5-layer thermal diffusion (TD) scheme (Dudhia, 1996) is a very elemental model, which basically only computes the temperature in the different soil layers. It does not include canopy, and soil moisture is read from a climatological table. The unified NOAH land surface model (Tewari et al., 2004) is more advanced, including canopy, root penetration depth, frozen soil, a layer of snow and surface runoff. It predicts values for soil moisture rather than reading area-averaged values from a lookup table.

The representation of soil moisture in mesoscale models becomes more and more important as the model resolution increases (Chen and Dudhia, 2001; Angevine et al., 2014) and we expect that this difference between the two surface schemes will be of substantial influence on the model results. Viterbo et al. (1999) highlighted the importance of the soil freezing feedback. Freezing of the top soil was often observed during KASCADE, which is another reason to expect better results from the runs with NOAH.

8

₂₆₁ Jin et al. (2010) compared four surface models of different complexity and found that simulation of most
₂₆₂ atmospheric variables improved with the complexity of the model.

₂₆₃ 3.3   PBL parameterization

₂₆₄ The PBL scheme computes the transport of heat, water vapor and momentum due to turbulent mixing.
₂₆₅ Considering only vertical transport and omitting overbars for mean variables (which we will do through-
₂₆₆ out this study), the contribution of turbulence to the rate of a change of any mean atmospheric variable
₂₆₇ C (e.g. momentum (U), heat (θ), specific humidity (q)) can be expressed as (Stull, 1988):

$$\frac{\partial C}{\partial t} = -\frac{\partial \overline{w'C'}}{\partial z} \ . \tag{1}$$

₂₆₈ The correlation term $\overline{w'c'}$ represents the turbulent flux. Since the model only computes the evolution of
₂₆₉ the mean flow, and not the perturbations terms w' and C' (Stensrud, 2007), this correlation term needs
₂₇₀ to be parameterized. There are several ways to do this, and we will briefly discuss the parameterization
₂₇₁ schemes that we used in this study.

₂₇₂ 3.3.1   Non-local closure

₂₇₃ The first two schemes are YSU (Hong et al., 2006) and ACM2 (Pleim, 2007), so-called first-order schemes,
₂₇₄ meaning that the turbulent term is directly related to the gradient of the considered variable C:

$$\overline{w'C'} = -K_C \frac{\partial C}{\partial z} \ , \tag{2}$$

₂₇₅ where K_C is the eddy diffusivity for C. However, based on the consideration that large eddies of the
₂₇₆ order boundary layer height account for an important part of the total energy transport, both schemes
₂₇₇ incorporate a non-local mixing term. In YSU, this is done by adding a so-called 'countergradient term'
₂₇₈ to the local approach. This term is proportional to the height above the surface and the transport rate
₂₇₉ at the surface. This results in

$$\frac{\partial C}{\partial t} = \frac{\partial}{\partial z} \left[K_C(\frac{\partial C}{\partial z} - \gamma_C) - \overline{(w'C')}_h (\frac{z}{h})^3 \right] \ , \tag{3}$$

₂₈₀ where we recognize the first-order closure in the first term on the right hand side (rhs). γ_C is the
₂₈₁ countergradient correction, and the last term represents entrainment at the boundary-layer top. ACM2
₂₈₂ uses another method to account for non-local fluxes called 'transilient turbulence theory'. This theory
₂₈₃ extends local closure as it suggests that the same method (eddy diffusivity times gradient) can be used

to compute the turbulent fluxes between the considered level and *any* other level, instead of only the two nearest neighbors. The choice of these levels is arbitrary. In ACM2, for any level, the total turbulent flux is a combination of the flux from the surface, the flux from the level immediately below and the flux to the level immediately above. In mathematical terms, this takes the form:

$$\frac{\partial C_i}{\partial t} = f \left(M^\uparrow C_1 - M_i^\downarrow C_i + M_{i+1}^\downarrow C_{i+1} \frac{\Delta z_{i+1}}{\Delta z_i} \right) + \frac{\partial}{\partial z} \left(K_C (1-f) \frac{\partial C}{\partial z} \right) \ , \tag{4}$$

where, again, first-order closure for local mixing can be recognized in the last term on the rhs. The other terms represent the transilient turbulence theory and the factor f determines the relative contributions of the local and non-local closure approach. For example, at night, $f = 0$ and only local closure is considered. $M^\uparrow$ and $M^\downarrow$ are up- and downward mixing rates, and Δz indicates the layer depth. The subscript i indicates the different vertical layers. The definition of K_C differs between the two models.

3.3.2 TKE-closure

Another commonly applied method to parameterize the turbulent transport terms in the governing equations is so-called 1.5-order or TKE-closure. We use three of these 1.5-order schemes in our study: MYJ (Janjic, 1994), MYNN2.5 (Nakanishi and Niino, 2006) and QNSE (Sukoriansky et al., 2005). In these schemes, extra prognostic equations are derived for mean turbulent kinetic energy (TKE) and for the mean variance of potential temperature and humidity. This results in more unknowns in the system of equations, but the inclusion of TKE provides extra information on the mixing characteristics. Whereas K_C was merely an empirical constant in the first order closure, it can now be a function of TKE, which results in more realistic turbulence intensity. Generally, this function takes the form of (Stensrud, 2007):

$$K_C = \lambda e^{0.5} \ , \tag{5}$$

where λ is a function of the height above the surface and the stability of the atmosphere, and e is the mean TKE. Again, the definitions of λ and hence K_C differ between the models. For details about the formulation of K_C the reader is referred to Stull (1988), Kleczek et al. (2014) or the original references for each scheme.

3.3.3 Review of previous PBL studies

Every PBL parameterization has its strong and weak points, and the choice for a specific scheme is dependent on the intended application and the specific case (summer/winter, strong/weak synoptic forcing, García-Díez et al. 2013). For example, Draxl et al. (2014) found good agreement between the

10

wind field produced with TKE schemes and their observations. Therefore, they recommended one of these schemes for their intended application in wind energy, even though ACM2 gave a better representation of the temperature profile. On the other hand, Hu et al. (2010) did a similar study with different PBL schemes, and found indeed that a TKE scheme produced higher wind speeds than the non-local schemes. However, the lower wind speeds forecast by YSU and ACM2 were closer to the observations in their case.

Even though there are large differences between PBL studies, there are some general findings that recur in literature. Non-local mixing schemes usually generate more entrainment, resulting in thicker, dryer and warmer PBLs (Bright and Mullen, 2002; García-Díez et al., 2013; Holtslag et al., 2013). On the other hand, TKE-closure schemes often outperform first-order closure schemes in the simulation of the stable boundary layer (Shin et al., 2012; Kleczek et al., 2014), because the decay of turbulence after sunset is more gradual and the local schemes are less sensitive to strong gradients near the ground. In the current version of WRF, YSU uses higher mixing under stable conditions (Hong and Kim, 2008; Hong, 2010). In the case of weakly stable boundary layers, this improves the simulated night time temperature and moisture profiles. However, under very stable conditions, this extra mixing is not desirable.

García-Díez et al. (2013) performed an extensive seasonal evaluation of three of the PBL schemes used in this study: YSU, ACM2 and MYJ. They found a cold bias in summer and a warm bias in winter. The diurnal temperature range was underestimated throughout the year. PBL growth is usually underestimated in all schemes, except for YSU when the PBL depth is below 1000m. This is not the case in the current study, so we anticipate the same underestimation for all schemes in our results. A specific case from their study was analyzed in more detail, and it was found that turbulent fluxes were overestimated. The authors state that the biases in temperature and DTR can only arise from errors in the radiation balance, but encourage that further research is carried out to confirm this.

Overestimation of turbulent fluxes has also been reported by other authors, e.g. Steeneveld et al. (2011). At the same time, the closure problem in energy balance observations remains a challenge, especially under stable conditions (Zeng et al., 2012; Bosveld et al., 2014). Thus, the overestimation of fluxes by the model should be weighed against the reliability of the measurements.

Flows in SBLs are often anisotropic and internal waves occur frequently. In this situation, the physical reasoning on which K_C is based in YSU, ACM2, MYJ and MYNN2.5 is not sound and their validity is limited. In the derivation of the QNSE scheme, a spectral analysis is used to distinguish the effects of internal waves and turbulence. Different dispersion relationships for waves and turbulence are derived, dependent on the stability of the atmosphere. Based on this, new eddy diffusivities are formulated and applied to the PBL parameterization. Therefore, QNSE is expected to give better results in very stable situations. This is supported by a case study carried out by the developers (Sukoriansky et al., 2005). However, at day time the model can still produce large biases (Shin and Hong, 2011).

Some of the previous studies pointed to the importance of land-surface-atmosphere coupling (Shin et al., 2012; Zeng et al., 2012; Holtslag et al., 2013). For example, Shin et al. (2012) did an interesting study comparing the sensitivity of different PBL schemes to the height of the lowest model level. In SBLs, the gradient between the lowest model level and the surface varies considerably with the height of the lowest model level. The surface-layer parameterization is usually calculated between the surface and this lowest model level. It was found that non-local mixing schemes are more sensitive to this parameter, because the mixing properties of this level are transported to all higher levels in these schemes.

Based on all these previous findings, we may expect that the stable conditions that dominate our case are better simulated by the TKE-closure schemes, especially QNSE, and we expect that the model will have difficulties representing the large diurnal temperature range.

4 Results

4.1 Evaluation of reference schemes

In our discussion of the results, we will begin with the vertical profiles of potential temperature and mixing ratio (figure 5). Instantaneous profiles immediately give insight in the structure of the atmosphere while retaining more detail than interpolated graphs as in figure 3. Moreover, they allow for easy comparison of different model runs. We present the profiles at 12:00 UTC (19 February) and 06:00 UTC (20 February), because they represent two extreme states of the PBL: a well-defined mixed layer with maximum temperature versus a cold, stably stratified boundary layer. Later, we will present the temporal evolution of other diagnostic variables such as radiation and fluxes and we will discuss how they can explain the characteristics of the profiles shown here.

In the profiles of 12:00 UTC, we recognize again the PBL height of about 1400 m, and we see that the model fails to reproduce this mixed-layer height and the strong inversion marking its top. The configuration with NOAH+ACM2 performs better than the other configurations on this aspect. Following the profiles throughout the simulation (not shown), we find that the model *does* simulate advection, but there is a delay with respect to the measurements. This explains why at 12:00 UTC, above 1400 meter, the profiles from the model are colder and moister than observed. Also the mixed layer is 2 - 3 °C too cold and at least 1 gkg^{-1} too moist in the model. This could be due to a too small (large) sensible (latent) heat flux and/or too little warm/dry-air entrainment at the PBL-top. Both are intimately connected with the underestimation of PBL height (Van Heerwaarden et al., 2009). With the TD scheme, skin temperature is highly underestimated and the cold and moist biases in the PBL are larger than in NOAH.

12

At 06:00 UTC, we can distinguish several layers. Between the surface and 200 m, there is a strong temperature stratification. Between 200 and 450 m, the stratification is near neutral and between 450 and 600 meter we find another strong inversion. This pattern repeats itself once more. The model shows a similar layering, but it does not cool as much as in the measurements. The cooling near the surface is confined to a much too shallow layer (about 50 m). We note that there is a large gradient between the skin temperature and the temperature of the lowest model level. In section 4.2.1 we will investigate the role of the surface-layer scheme in this apparent lack of surface-atmosphere coupling. Advection is still underestimated by the model (not shown). The humidity profile shows a peak around 200 meter. We recall from figure 3D that the mixing ratio increased between 12:00 and 18:00 UTC over the full extent of the PBL, due to evapotranspiration. The peak value of 4 gkg^{-1} reflects this late-afternoon moisture content of the PBL. We infer that dew formation is responsible for the drying in the lower 200 m, while dry advection can explain the drying above 200 m. There is little difference between the model configurations. Only NOAH+QNSE is approximately 3 K colder and 0.5 gkg^{-1} dryer near the surface, as compared to the other runs. In the next section, we will link this to earlier decoupling of the lower atmosphere in this configuration.

In figure 6 we present a number of variables that can help us to understand the evolution of the PBL. We chose to show 110 m temperature rather than 2 meter temperature, because this variable is less sensitive to local effects that the model cannot simulate. As we can see, the DTR at this height is approximately 12 °C in the observations and only 7 °C in the model simulations. In figure 6B we read a net radiative cooling of about 60 Wm^{-2} from the observations, which is very high and typical for the development of a SBL. We find a bias in the longwave incoming radiation at the surface of about 20 Wm^{-2} and also the upward flux is underestimated. We note that there are some clouds in the beginning of the simulation that are not recognized by the model.

If we use the longwave outgoing radiation to compute the skin temperature according to the Stefan-Boltzmann law, we find peak values of 295 K for the 400 Wm^{-2} from the observation and 285 K for an average model value of 350 Wm^{-2}. Thus, an underestimation of the DTR of 10 °C! We can also use the Stefan-Boltzmann relationship to compute the longwave radiation at 110 meter. With an atmospheric emissivity of 0.8, this yields an underestimation of about 16 Wm^{-2} at noon. According to Bosveld et al. (2014), "50% of the longwave incoming radiation at the surface originates from the lower 200 m of the atmosphere." Assuming that the PBL is well mixed at noon, the bias at 110 m is a good representative for this layer, and it seems that at least part of the bias in longwave radiation can be attributed to a too cold atmospheric profile. Factors that could explain this cold bias are underestimation of advection or warm-air entrainment at the PBL top, or erroneous partitioning of the energy at the surface. We will explore the role of the surface in sections 4.2.1 and 4.2.3.

13

Continuing with figure 6C, we find that the 10-m wind speed is highly overestimated in the model. As a reference, we also plotted the observations at 110 meter. The general pattern of the wind is well reflected in the model, but it seems that the model does not experience enough drag near the surface. After sunset at 19 Feb, the wind speed at 110 m in the observations drops quickly, while the modelled wind at 110 m (not shown) remains strong ($\sim$10 ms^{-1}) until about 03:00 UTC. We attribute this drop in wind speed to the decay of turbulence and downward momentum transport. In figure 6D, we see that the friction velocity follows the same pattern and shows the same biases as the wind. In turn, friction velocity is used in the computation of other turbulent transport terms and we see the same errors propagating to the sensible and latent heat fluxes (figures 6E and F), with excessive mixing at noon and continuing after sunset till about 03:00 UTC. Concerning these heat fluxes, there is a difference between the two surface schemes, as NOAH predicts higher sensible heat fluxes while TD gives much higher latent heat fluxes. The latent heat flux is overestimated in both schemes, which could explain why the profile in figure 5C is too moist, and also why this bias was larger in the TD scheme. We will investigate the influence of soil moisture content on this bias in section 4.2.3. We inferred earlier that dew formation was responsible for the drying of the PBL at night, but we find that this is not measured by the sonic anemometers. De Roode et al. (2010) also found systematic drying trends in SBLs and discovered that dew formation is underestimated in flux calculations with the eddy-correlation technique. Here, we find analogous results as in their study.

4.2 Modification to the physics formulations

So far, we found that the model produces too wet and too shallow boundary layers, a too small DTR, a bias in longwave radiation, and overestimation of the wind and turbulent mixing. We found marginal difference between the model results from the various boundary-layer parameterizations. With respect to the land-surface parameterization, NOAH seems to give more realistic results than the TD scheme, mainly due to the excessive evapotranspiration of the latter. Hence we decide to continue our research with only one model configuration, namely NOAH+YSU, which is a commonly used configuration in modelling studies. Following the rationale that improving the structure of the PBL (vertical profiles of temperature and mixing ratio, PBL height and the DTR) might also improve the representation of the wind, we will perform sensitivity tests regarding surface coupling and radiation schemes, and we will investigate the influence of soil moisture.

4.2.1 Sensitivity to land-atmosphere coupling within the surface-layer scheme

Previous studies (e.g. Chen et al. (1997, 2010); Tastula (2014)) have emphasized the role of surface layer coupling in land-atmosphere models. The choice for $z_{0,t}$, representing the roughness length for heat, is found to be of major importance. Following Stensrud (2007), we will first show where this parameter occurs in the surface-layer parameterization.

The turbulent flux for heat H, is dependent on the temperature gradient between the surface T_s and the atmosphere T_a, and on the aerodynamic resistance r_H:

$$H = \frac{\rho c_p (T_s - T_a)}{r_H} \ , \tag{6}$$

where H represents the sensible heat flux, ρ the density of the air, c_p the specific heat capacity of the air. r_H is usually calculated with the logarithmic wind profile and a correction for non-neutral conditions, based on similarity theory:

$$r_H = \frac{1}{\kappa u_*} \left[ln(\frac{z_{eff}}{z_0}) - \Psi_h(\frac{z_{eff}}{L}) \right] \ , \tag{7}$$

where z_{eff} is the considered height (usually the first model level), κ is the van Karman constant (0.4) u_* is the friction velocity and L is the Obukhov-length. z_0 is the roughness length for momentum and is interpreted as the level at which the wind speed goes to zero. However, there is an additional resistance for heat transport, that originates from the consideration that heat transfer between the surface and z_0 must be governed by molecular diffusion, which is a much less efficient process than turbulent transport. Note that momentum transport in this so-called viscous sublayer can occur through pressure perturbation. For heat, however, no such mechanism exits. Therefore, an additional resistance is usually added through an extra term in the dominator of equation 7:

$$r_H = \frac{1}{\kappa u_*} \left[ln(\frac{z_{eff}}{z_0}) - \Psi_h(\frac{z_{eff}}{L}) + ln(\frac{z_0}{z_{0h}}) \right] \ , \tag{8}$$

If z_{0h} is equal to z_0, molecular diffusion is effective up to z_0 and there is no extra resistance. If z_{0h} is much smaller than z_0, there is a large extra resistance because neither turbulence nor molecular diffusion is effective in the layer between z_0 and z_{0h}. Numerous parameterizations for z_{0h} have been proposed in literature. It should, for example, be related to flow characteristics (Chen et al., 1997) or canopy height (Chen and Zhang, 2009). A commonly used formulation is that of Zilitinkevich (1995):

$$\frac{z_0}{z_{0h}} = \exp(\kappa C_{zil} Re*^{0.5}) \ , \tag{9}$$

where $Re*$ is the roughness Reynolds number and C_{zil} is an empirical coefficient. The Zilitinkevich

15

coefficient is reported to vary between 0.01 (large z_{0h}, strong coupling) and 1.0 (small z_{0h}, weak coupling) (Trier et al., 2011). Chen and Zhang (2009) proposed a canopy-dependent C_{zil}, which is also incorporated in the default surface layer scheme for YSU. Yang et al. (2008), hereafter Y08, and Chen et al. (2010) proposed an alternative formulation where they related z_{0h} to a physical height through empirical relations, which in their case resulted in better representation of skin temperature and heat fluxes:

$$z_{0h} = \frac{70\nu}{u_*} \exp(-7.2u_*^{0.5}|T_*|^{0.25}) \, , \tag{10}$$

where ν is the molecular viscosity of the air and T_* is a non-dimensional temperature scale defined as $-\overline{w'T'}/u_*$.

We test the sensitivity of our model to the surface coupling strength by changing the Zilitinkevich coefficient to the limits of its reported range (0.01 and 1.0) and we ran a simulation with the canopy dependent formulation. Also, we tested the formulation of Y08. Finally, we ran the model with a revised surface layer formulation of Jiménez et al. (2012). The revisions explained in this paper should improve the similarity functions under stable conditions. Furthermore, a modification is made that makes the use of enforced limitations (in figure 6D, e.g., u_* is limited to 0.1 ms^{-1}) unnecessary.

The result of our experiments are summarized in table 3. Here, we evaluate the variables that we find most suitable to illustrate the models behaviour (and shortcomings). Following Taylor (2001), we show the root mean square difference split up in a centered part and a mean overall bias, correlation coefficient and normalized variance. Variance expresses the spread around the mean, which for variables that exhibit a diurnal cycle, can be interpreted as a measure for the amplitude of this daily variation. The solutions of the canopy-dependent C_{zil} (not shown) were slightly unstable, and otherwise similar to strong coupling ($C_{zil} = 0.01$).

We find that strong surface coupling improves wind and temperature profiles, but at the cost of skin temperature (through $LW \uparrow$) and sensible and latent heat fluxes, and vice versa. The peak of H at noon is 190 Wm^{-2} in the strong coupling run versus 145 Wm^{-2} in the measurement; in the weak coupling, it is only 75 Wm^{-2}. For the latent heat flux, these values are 125, 50 and 40 Wm^{-2} and the peak values of $LW \uparrow$ are 340, 400 and 420 Wm^{-2}, respectively. In the strong coupling run, we find stronger dew formation at night. Y08 gives a better representation of the sensible heat flux but some correlation with especially the wind pattern is lost. Hence, we do not consider this scheme as a general improvement to the model performance. Finally, we find that the revised surface layer scheme differs only slightly from the original scheme, but as its physical basis is more complete, we decide to retain this surface layer scheme in our following simulations.

To illustrate the influence of the coupling strength on the PBL-structure, we present figure 7. The

difference in temperature at noon between the extremes of C_{zil} is approximately 1 °C. Humidity varies by about 0.5 gkg^{-1}. Weaker surface coupling results in a shallower PBL and weaker inversion at noon. The stronger coupling only marginally affects the model results at that time. At night, the profile is slightly colder with stronger coupling, but what is most striking is the improved resemblance of the humidity profile at 06:00 UTC. We now recognize the peak that we also saw in the measurements, which is directly linked to higher dew formation at night (not shown). The peak value of almost 4.5 gkg^{-1} again resembles the humidity of the mixed layer at 18:00 UTC. As the latent heat flux is also amplified by the stronger coupling, this value is now too high.

Stronger surface coupling thus results in larger heat fluxes at daytime. This improves the boundary-layer growth and simulation of wind and temperature profiles, but deteriorates the representation of sensible and latent heat fluxes and of skin temperature. It enhances the formation of dew, but also increases the overall bias in specific humidity. Altogether, we are not satisfied with these results and we continue our investigation. In the next section, we test the sensitivity of the model to the radiation parameterization.

4.2.2 Sensitivity to selected radiation scheme

We found a strong bias in the representation of surface longwave radiation fluxes. As noted in section 4.1 this bias can at least partly be explained by the too cold atmosphere. However, insufficient heating of the atmosphere can also be a *result* of the too small radiative forcing. This positive feedback mechanism makes it difficult to identify the source of the biases. In previous studies, it was found that the radiation scheme can have significant influence on the model results (Iacono and Nehrkorn, 2010; Seefeldt et al., 2012; Karlickỳ, 2013). To assess the influence of the radiation scheme on our simulation, we test 3 alternative radiation configurations: Goddard shortwave (Chou and Suarez, 1994) and RRTM longwave, CAM (Collins et al., 2004) shortwave and longwave , and RRMTG (Iacono et al., 2008) shortwave and longwave (figure 8).

It appears that the simulation using CAM radiation does simulate the clouds that were observed early in IOP15. The other schemes fail to reproduce these clouds. However, the $LW \downarrow$ bias in the CAM simulation is larger than in the other schemes. The configuration with RRTMG slightly improves the overall bias in longwave downward radiation (-15.85 versus -18.47 Wm^{-2} in the reference run). However, the maximum difference is still 20 Wm^{-2}. We also computed the statistics for these runs (not shown). Overall, longwave radiation components and T110 improve slightly for the configurations with Goddard and with RRMTG, but this does not improve the representation of the other variables. In fact, the bias in most variables becomes larger. We conclude we can not improve the overall model performance by changing the radiation parameterization. However, using RRTMG gives slightly better results for the

representation of longwave radiation, so we decide to stick with this scheme for the final simulations.

4.2.3 Influence of soil moisture

We noted in section 4.1 that evaporation is too high and the vertical profile is too moist. A possible cause could be too high soil moisture values in initial conditions that we used. Unfortunately, we have no measurements of soil moisture to support this hypothesis, but it is true that the soils are generally dry in this area, and hence it would not be surprising if soil moisture is too high in the boundary conditions.

The important role of soil moisture in mesoscale modelling was recently emphasized in Angevine et al. (2014). Both the latent heat flux and the soil heat conductivity are dependent on soil moisture. Lower soil moisture would result in a lower soil conductivity, lower evapotranspiration and thus a larger skin temperature and a larger sensible heat flux. In turn, a larger H would result in more boundary layer growth and a warmer mixed layer (Van Heerwaarden et al., 2009). To assess the influence of the soil moisture in our simulation, we manually reduced the soil moisture field in the surroundings of Cadarache by half.

The results are shown in figure 9. In E) and F), we see immediately that the reduction of soil moisture has a large influence on the partitioning of the heat fluxes. LvE is now underestimated by more than $20 \, \mathrm{Wm^{-2}}$, while H is overestimated by $120 \, \mathrm{Wm^{-2}}$. Like we saw earlier in the run with stronger surface coupling, this higher H results in a higher PBL and a stronger inversion. The PBL is ~0.2 $\mathrm{gkg^{-1}}$ dryer at noon, but at night there is little difference. Dew formation is not enhanced, like it was in the run with stronger coupling. While the temperature profile and DTR improved by ~1 °C, the wind at 10 and 110 m is not much influenced by the soil moisture change. Skin temperature at noon is even a bit overestimated.

By reducing the soil moisture. We have found again that a larger sensible heat flux improves the model vertical structure of the atmosphere and the diurnal temperature range. However, to obtain a PBL height that corresponds to the observations would require an H that cannot be justified with the measurements, even if a very large uncertainty is accounted for. Thus, there must be another process that the model fails to represent. Possibly, this has to do with the interaction of the PBL and the warm/dry advection, or the representation of the wind profile.

4.3 Final result of modelling efforts

We close our study with the modelled evolution of wind, temperature and humidity (figure 10). It complements the KASCADE data as shown in figure 3 because of its higher temporal resolution (10 minutes), and it allows us to present a final assessment of the models performance and shortcomings

that we have identified through this study.

The general pattern of the wind is well-captured by the model. Only in the first hours of spin-up, the simulated wind direction is a bit too much from the east, and on 20 February, the north-northeast component appears too late. Wind speeds are overestimated on 19 February and do not decrease until ~03:00 UTC, while the observed wind speed decreases already around sunset. We linked this to the decay of turbulence and lack of downward momentum transport, associated with the evening transition.

Even though we noted in section 4.1 that advection is somewhat delayed in the model, figure 10C demonstrates that the general pattern of advection is rather well simulated. For example, if we follow the 288 K isentrope, we find that it lowers to approximately 1000 m during the simulation, just like in the measurements. However, the strong temperature gradient that we find in the measurements is smoothed in the model simulation. This may be correlated with the underestimated PBL height in the model. We also find that the diurnal variation of temperature (DTR) and humidity in the model is not as large as in the measurements. Dew formation at night is not well-represented by the model and overall values for specific humidity are overestimated.

5 Discussion

The model has most difficulties during boundary-layer growth and decay. There is too little boundary-layer growth, and the mixed-layer height is underestimated. Possibly, there is an underestimation of dry air entrainment at the PBL top. After sunset, downward momentum transport continues for much too long (3 hours at least), resulting in too high wind speeds, mixing and not enough cooling/stratification near the surface. Possibly, this prevents decoupling of the lower, stably stratified layer and the formation of local flows.

Previous studies have already revealed that mesoscale models as well as single-column models and large-eddy simulation models struggle to correctly reproduce the transition from a daytime convective mixed-layer to a night time stable regime (Basu et al., 2008; Svensson et al., 2011; Bosveld et al., 2014). This transition has been thoroughly investigated during the BLLAST-campaign (Lothon et al., 2014) and currently, model studies are being carried out to address this modelling issue (e.g. Sastre Marugán et al. (2013); Jimenez et al. (2014)).

We have found that our model results are not always in agreement with the KASCADE measurements. One of the reasons may lie in the representation of the terrain in the model. As noted by Jiménez and Dudhia (2012), the impact of unresolved topographic effects on the model results can be substantial. They also highlighted the importance of selecting a representative grid cell to compare with the observations. We have tested the sensitivity of the model to this grid-cell choice by selecting different grid cells close

to the measurement locations and found marginal differences between the model output. However, we noted that most of the measurements during the KASCADE campaign were carried out in a small valley, which the model does not resolve on a 1-km resolution. This valley may affect the lower ~150 m of the measured atmospheric profiles through sheltering of the wind and the accumulation of cold air due to drainage flows inside the valley. This could explain, for example, why the model does not reproduce the strong nocturnal cooling in the lower 200 meters (figure 5B).

Unfortunately, no observations of the soil heat flux were available and we could not check the closure of the energy balance. However, using a simple empirical formula from De Rooy and Holtslag (1999), we related the ground heat flux to the observations of 2-meter temperature. Using these estimates, we found that the energy balance does not close. For example at noon, the energy available at the surface $(Q^* - G)$ is 100 Wm^{-2} larger than the energy that is used for heating and evapotranspiration $(H + LvE)$. This non-closure of the observed energy balance reinforces our rationale that a larger H is required to explain the observed boundary-layer height and DTR. On the other hand, to achieve perfect correspondence of the modelled profile with the observations would require an H that is even (much) larger than 100 Wm^{-2} and we suspect that other processes, for example entrainment, play a role as well.

We used the ECMWF operational analysis data as initial and boundary conditions. To check the sensitivity of the model to these input fields, we also ran a simulation with analysis data from the National Center for Environmental Prediction (NCEP) Global Forecasting System (GFS). These initial fields turned out to contain a snow layer which was not there at the time of the measurements, nor shortly before the measurements were taken. This layer of snow caused changes in albedo and net radiation, resulting in lower sensible heat fluxes (50 Wm^{-2} compared to 145 Wm^{-2} in the observations). In turn, the model predicted less boundary layer growth, lower temperatures and a smaller DTR. This unrealistic snow layer in the GFS initial fields is found more often in the daily operational forecasts run at Cadarache (T. Heddde, personal communication, 24 October 2014). Our results show that it has a substantial impact on the model results and we advise to circumvent such erroneous initial fields as much as possible.

Currently, model studies are being performed concerning the afternoon transition (related to BLLAST, (Lothon et al., 2014)), cold pooling (related to the COLd Pooling EXperiment, COLPEX, (Price et al., 2011)) and high resolution modelling in general (High Resolution modelling in Complex Terrain, HiRCoT, (Arnold et al., 2012)), and the first promising results have recently been published (Vosper et al., 2013; Angevine et al., 2014). They report, respectively, that the influence of vertical resolution on the model results is large in areas of complex terrain, and that an innovative technique to improve the spatial representation of soil moisture can substantially improve the model results. Future studies may benefit from these new insights.

6 Summary and conclusions

Stable boundary layer formation and complex terrain are both difficult to understand and represent in atmospheric models. Channeled winds, cold-pool formation, elevated valley inversions, katabatic winds and flow decoupling are only a few of the phenomena that characterize the complex atmospheric behaviour imposed by these conditions. At the same time, these conditions form the largest threat in case of incidental release of effluents, because dispersion is limited by the stable stratification.

We studied a case in southeastern France, where stable conditions occur frequently. The area is further characterized by a large diurnal temperature range and is generally very dry. At Cadarache, a nuclear research centre located in the area, the extensive measurement campaign 'KASCADE' has been carried out in 2013 to facilitate future impact studies. We used this data set to evaluate the performance of the WRF meteorological model. In turn, the model output will complement the KASCADE measurements.

We used four nested domains to represent the 100*100 km area surrounding Cadarache with a high resolution of 1 km. We ran a simulation of 48 hours, covering two stable, but contrasting nights that where both intensively observed during the KASCADE campaign. The first night was characterized by weak winds (4 ms^{-1}) and jet formations in the lower 1000 m, with directions along the axis of the Durance valley. The second night showed much stronger winds (up to 15 ms^{-1}) and less clear wind channeling through the valley. During the full simulation period, dry and warm air was advected between 1000 and 2000 m from the northeast. We ran the model with 5 different pbl schemes and 2 different surface parameterizations (table 2).

The model highly underestimates the diurnal temperature range. Convective boundary layers are too shallow and the capping inversions are not sharp enough. Advection is simulated by the model, but not as strong as in the measurements. We found little difference between the different pbl parameterizations. NOAH predicted better skin temperatures than the MM5 5-layer thermal diffusion scheme. With both schemes, evaporation is overestimated, but to a much larger extent in the thermal diffusion scheme. Also, we found a bias in the incoming longwave radiation as large as -18.5 Wm^{-2}.

We then took a commonly used configuration in WRF studies, NOAH+YSU, and tested its sensitivity to the strength of atmosphere-surface coupling by varying the Zilitikevich parameter C_{zil}. With very strong coupling, we found more realistic dew formation at night. Also, the shape of the temperature profile improved with stronger coupling at daytime, with higher mixed layer and stronger inversion, although this was only a very minor improvement with respect to the original simulation. At the same time, sensible and latent heat fluxes were even more overestimated, at the cost of the diurnal range of skin temperatures.

In a sensitivity study to the role of the radiation scheme, we learnt that using the CAM scheme for

both longwave and shortwave radiation parameterization, results in a larger bias. However, it was the only scheme that recognized the formation of some clouds in the very beginning of the simulation. The other options (Goddard Shortwave and RRTMG long- and shortwave) showed very small improvements in the incoming longwave radiation, but still, the bias was -16 Wm^{-2}.

Finally, we reduced the soil moisture content in the model. This resulted in a higher mixed layer, stronger capping inversion and a slightly drier vertical profile. Still the model boundary layer was about 400 m too low and 1 gkg^{-1} too moist and the costs for the sensible heat flux were proportional (135 Wm^{-2} larger than in the measurements).

Overall, the model was able to predict large scale wind speed and direction to a good extent. Advection was also simulated, although not strong enough. Within the PBL, the evolution of most variables follows the right pattern, but the diurnal range of temperature and humidity is underestimated, while the turbulent fluxes are overestimated.

The next step in the context of KASCADE modelling studies is to generalize our results for other IOPs. Future studies can than proceed in two directions. The first direction is to use the current model results to study the local flow patterns like the Durance valley wind, taking into consideration the model deficiencies that we identified in this study. Such studies would largely contribute to the understanding of valley winds, cold pooling and boundary layer evolution over complex terrain in general and specifically to the understanding of the complex atmospheric behaviour in the Durance valley. The other path is to try and further improve the model performance. These studies will probably benefit from increasing the vertical resolution and the spatial distribution of soil moisture. Also, they need to account for the inconvenient effect that the small Cadarache valley has had on the KASCADE measurements.

Acknowledgments

References

Angevine, W., E. Bazile, D. Legain, and D. Pino, 2014: Land surface spinup for episodic modeling. *Atmospheric Chemistry and Physics Discussions*, **14 (4)**, 4723–4744.

Arnold, D., et al., 2012: *High resolution modelling in complex terrain: report on the HiRCoT 2012 Workshop, Vienna, 21-23 February 2012*. Institut für Meteorologie, Department Wasser-Atmosphäre-Umwelt, Univ. f. Bodenkultur, 42 pp.

Arnold, D., et al., 2014: Issues in high-resolution atmospheric modeling in complex topography–the HiRCoT workshop. *Hrvatski meteorološki časopis*, **47 (47)**, 3–11.

Basu, S., J.-F. Vinuesa, and A. Swift, 2008: Dynamic les modeling of a diurnal cycle. *Journal of Applied Meteorology and Climatology*, **47 (4)**, 1156–1174.

Bosveld, F. C., et al., 2014: The third gabls intercomparison case for evaluation studies of boundary-layer models. part b: results and process understanding. *Boundary-Layer Meteorology*, 1–31.

Bright, D. R. and S. L. Mullen, 2002: The sensitivity of the numerical simulation of the southwest monsoon boundary layer to the choice of pbl turbulence parameterization in mm5. *Weather and Forecasting*, **17 (1)**, 99–114.

Brutsaert, W., 1972: Radiation, evaporation and the maintenance of turbulence under stable conditions in the lower atmosphere. *Boundary-Layer Meteorology*, **2 (3)**, 309–325.

Büttner, G., J. Feranec, G. Jaffrain, C. Steenmans, A. Gheorghe, and V. Lima, 2002: Corine land cover update 2000. *Technical guidelines. Copenhagen, Denmark: European Environment Agency.*

Carrera, M. L., J. R. Gyakum, and C. A. Lin, 2009: Observational study of wind channeling within the st. lawrence river valley. *Journal of Applied Meteorology and Climatology*, **48 (11)**, 2341–2361.

Chen, F. and J. Dudhia, 2001: Coupling an advanced land surface-hydrology model with the penn state-ncar mm5 modeling system. part i: Model implementation and sensitivity. *Monthly Weather Review*, **129 (4)**, 569–585.

Chen, F., Z. Janjić, and K. Mitchell, 1997: Impact of atmospheric surface-layer parameterizations in the new land-surface scheme of the ncep mesoscale eta model. *Boundary-Layer Meteorology*, **85 (3)**, 391–421.

Chen, F. and Y. Zhang, 2009: On the coupling strength between the land surface and the atmosphere: From viewpoint of surface exchange coefficients. *Geophysical Research Letters*, **36 (10)**.

23

Chen, Y., K. Yang, D. Zhou, J. Qin, and X. Guo, 2010: Improving the noah land surface model in arid regions with an appropriate parameterization of the thermal roughness length. *Journal of Hydrometeorology*, **11 (4)**, 995–1006.

Chou, M.-D. and M. J. Suarez, 1994: An efficient thermal infrared radiation parameterization for use in general circulation models. *NASA Tech. Memo*, **104606 (3)**, 85.

Collins, W. D., et al., 2004: Description of the NCAR community atmosphere model (CAM 3.0). Technical Note TN-464+ STR, National Center for Atmospheric Research, Boulder, CO, 214 pp.

Cuxart, J., M. Jiménez, and D. Martínez, 2007: Nocturnal meso-beta basin and katabatic flows on a midlatitude island. *Monthly weather review*, **135 (3)**, 918–932.

De Meij, A. and J. Vinuesa, 2014: Impact of srtm and corine land cover data on meteorological parameters using wrf. *Atmospheric Research*, **143**, 351–370.

De Roode, S. R., F. C. Bosveld, and P. S. Kroon, 2010: Dew formation, eddy-correlation latent heat fluxes, and the surface energy imbalance at cabauw during stable conditions. *Boundary-layer meteorology*, **135 (3)**, 369–383.

De Rooy, W. C. and A. Holtslag, 1999: Estimation of surface radiation and energy flux densities from single-level weather data. *Journal of Applied Meteorology*, **38 (5)**, 526–540.

Draxl, C., A. N. Hahmann, A. Peña, and G. Giebel, 2014: Evaluating winds and vertical wind shear from weather research and forecasting model forecasts using seven planetary boundary layer schemes. *Wind Energy*, **17 (1)**, 39–55.

Draxler, R. and G. Rolph, 2003: Hysplit (hybrid single-particle lagrangian integrated trajectory) model access via noaa arl ready website (http://www.arl.noaa.gov/ready/hysplit4.html). noaa air resources laboratory, silver spring. Md.

Dudhia, J., 1989: Numerical study of convection observed during the winter monsoon experiment using a mesoscale two-dimensional model. *Journal of the Atmospheric Sciences*, **46 (20)**, 3077–3107.

Dudhia, J., 1996: A multi-layer soil temperature model for mm5. *Preprint from the Sixth PSU/NCAR Mesoscale Model Users' Workshop*, 22–24.

Duine, G.-J., P. Durand, T. Hedde, P. Roubin, P. Augustin, M. Fourmentin, F. Lohou, and M. Lothon, 2014a: Observations of radiation divergence and stability driven slope flows during the field experiment kascade. *EGU General Assembly Conference Abstracts*, Vol. 16, 1640.

Duine, G.-J., et al., 2014b: Stable boundary layer characterization in an orographic complex region: the field measurement campaign kascade. *21st Symposium on Boundary Layers and Turbulence, Leeds UK, June 09-13, 2014*, 8B.2, URL https://ams.confex.com/ams/21BLT/webprogram/Paper245848.html.

Ganteaume, A., J. Marielle, L.-M. Corinne, C. Thomas, and B. Laurent, 2009: Fuel characterization and effects of wildfire recurrence on vegetation structure on limestone soils in southeastern france. *Forest ecology and management*, **258**, S15–S23.

García-Díez, M., J. Fernández, L. Fita, and C. Yagüe, 2013: Seasonal dependence of wrf model biases and sensitivity to pbl schemes over europe. *Quarterly Journal of the Royal Meteorological Society*, **139 (671)**, 501–514.

Holtslag, A., et al., 2013: Stable atmospheric boundary layers and diurnal cycles: challenges for weather and climate models. *Bulletin of the American Meteorological Society*, **94 (11)**, 1691–1706.

Hong, S.-Y., 2010: A new stable boundary-layer mixing scheme and its impact on the simulated east asian summer monsoon. *Quarterly Journal of the Royal Meteorological Society*, **136 (651)**, 1481–1496.

Hong, S.-Y. and S.-W. Kim, 2008: Stable boundary layer mixing in a vertical diffusion scheme. *Proc. Ninth Annual WRF User's Workshop*, Boulder, CO, 3.3, URL http://www.mmm.ucar.edu/wrf/users/workshops/WS2008/abstracts/3-03.pdf.

Hong, S.-Y. and J.-O. J. Lim, 2006: The wrf single-moment 6-class microphysics scheme (wsm6). *J. Korean Meteor. Soc*, **42 (2)**, 129–151.

Hong, S.-Y., Y. Noh, and J. Dudhia, 2006: A new vertical diffusion package with an explicit treatment of entrainment processes. *Monthly Weather Review*, **134 (9)**, 2318–2341.

Hu, X.-M., J. W. Nielsen-Gammon, and F. Zhang, 2010: Evaluation of three planetary boundary layer schemes in the wrf model. *Journal of Applied Meteorology and Climatology*, **49 (9)**, 1831–1844.

Iacono, M. and T. Nehrkorn, 2010: Assessment of radiation options in the advanced research wrf weather forecast model. *Proceedings of 1st atmospheric system research science team meeting, Bethesda, MD, Office of Science, US Department of Energy*, 15–19.

Iacono, M. J., J. S. Delamere, E. J. Mlawer, M. W. Shephard, S. A. Clough, and W. D. Collins, 2008: Radiative forcing by long-lived greenhouse gases: Calculations with the aer radiative transfer models. *Journal of Geophysical Research: Atmospheres (1984–2012)*, **113 (D13)**.

Janjic, Z. I., 1994: The step-mountain eta coordinate model: Further developments of the convection, viscous sublayer, and turbulence closure schemes. *Monthly Weather Review*, **122 (5)**, 927–945.

Jimenez, M. A., W. M. Angevine, E. Bazile, F. Couvreux, J. Cuxart, D. Pino, and M. Sastre, 2014: An intercomparison of mesoscale simulations during the boundary layer late afternoon and sunset turbulence (bllast) experimental field campaign. *EGU General Assembly Conference Abstracts*, Vol. 16, 1629.

Jiménez, P. A. and J. Dudhia, 2012: Improving the representation of resolved and unresolved topographic effects on surface wind in the wrf model. *Journal of Applied Meteorology and Climatology*, **51 (2)**, 300–316.

Jiménez, P. A., J. Dudhia, J. F. González-Rouco, J. Navarro, J. P. Montávez, and E. García-Bustamante, 2012: A revised scheme for the wrf surface layer formulation. *Monthly Weather Review*, **140 (3)**, 898–918.

Jin, J., N. L. Miller, and N. Schlegel, 2010: Sensitivity study of four land surface schemes in the wrf model. *Advances in Meteorology*, **vol. 2010**, 11 pages, doi:10.1155/2010/167436, article ID 167436.

Kain, J. S., 2004: The kain-fritsch convective parameterization: an update. *Journal of Applied Meteorology*, **43 (1)**, 170–181.

Karlickỳ, J., 2013: Regional climate simulations with wrf model. *WDS'13 Proceedings of Contributed Papers: Part III Physics*, 80–84.

Kleczek, M. A., G.-J. Steeneveld, and A. A. Holtslag, 2014: Evaluation of the weather research and forecasting mesoscale model for gabls3: Impact of boundary-layer schemes, boundary conditions and spin-up. *Boundary-Layer Meteorology*, **152 (2)**, 213–243.

Kondo, J., O. Kanechika, and N. Yasuda, 1978: Heat and momentum transfers under strong stability in the atmospheric surface layer. *Journal of the Atmospheric Sciences*, **35 (6)**, 1012–1021.

Lothon, M., et al., 2014: The bllast field experiment: Boundary-layer late afternoon and sunset turbulence. *Atmospheric Chemistry and Physics*, **14 (20)**, 10 931–10 960.

Mahrt, L., 1999: Stratified atmospheric boundary layers. *Boundary-Layer Meteorology*, **90 (3)**, 375–396.

Mahrt, L., 2014: Stably stratified atmospheric boundary layers. *Annual Review of Fluid Mechanics*, **46 (1)**, 23–45.

Manins, P., 1992: Vertical fluxes in katabatic flows. *Boundary-layer meteorology*, **60 (1-2)**, 169–178.

26

Manins, P. and B. Sawford, 1979: Katabatic winds: A field case study. *Quarterly Journal of the Royal Meteorological Society*, **105 (446)**, 1011–1025.

Medeiros, L. E. and D. R. Fitzjarrald, 2014: Stable boundary layer in complex terrain. part i: Linking fluxes and intermittency to an average stability index. *Journal of Applied Meteorology and Climatology*, **53 (9)**, 2196–2215.

Mlawer, E. J., S. J. Taubman, P. D. Brown, M. J. Iacono, and S. A. Clough, 1997: Radiative transfer for inhomogeneous atmospheres: Rrtm, a validated correlated-k model for the longwave. *Journal of Geophysical Research: Atmospheres (1984–2012)*, **102 (D14)**, 16 663–16 682.

Nakanishi, M. and H. Niino, 2006: An improved Mellor–Yamada level-3 model: Its numerical stability and application to a regional prediction of advection fog. *Boundary-Layer Meteorology*, **119 (2)**, 397–407.

Pleim, J. E., 2007: A combined local and nonlocal closure model for the atmospheric boundary layer. part i: Model description and testing. *Journal of Applied Meteorology and Climatology*, **46 (9)**, 1383–1395.

Poulos, G. S., et al., 2002: Cases-99: A comprehensive investigation of the stable nocturnal boundary layer. *Bulletin of the American Meteorological Society*, **83 (4)**, 555–581.

Price, J., et al., 2011: Colpex: field and numerical studies over a region of small hills. *Bulletin of the American Meteorological Society*, **92 (12)**, 1636–1650.

Sastre Marugán, M., G.-J. Steeneveld, C. Yagüe, C. Román-Cascón, G. Maqueda, and A. van de Boer, 2013: WRF simulations of the atmospheric boundary layer evening transitions during the BLLAST field campaign. *EGU General Assembly Conference Abstracts*, EGU General Assembly Conference Abstracts, Vol. 15, 623.

Seefeldt, M. W., M. Tice, J. J. Cassano, and M. D. Shupe, 2012: Evaluation of wrf radiation and microphysics parameterizations for use in the polar regions. *AGU Fall Meeting Abstracts*, Vol. 1, 0091.

Shin, H. H. and S.-Y. Hong, 2011: Intercomparison of planetary boundary-layer parametrizations in the wrf model for a single day from cases-99. *Boundary-Layer Meteorology*, **139 (2)**, 261–281.

Shin, H. H., S.-Y. Hong, and J. Dudhia, 2012: Impacts of the lowest model level height on the performance of planetary boundary layer parameterizations. *Monthly Weather Review*, **140 (2)**, 664–682.

Skamarock, W. C. and J. B. Klemp, 2008: A time-split nonhydrostatic atmospheric model for weather research and forecasting applications. *Journal of Computational Physics*, **227 (7)**, 3465–3485.

Steeneveld, G., L. Tolk, A. Moene, O. Hartogensis, W. Peters, and A. Holtslag, 2011: Confronting the wrf and rams mesoscale models with innovative observations in the netherlands: evaluating the boundary layer heat budget. *Journal of Geophysical Research: Atmospheres (1984–2012)*, **116 (D23)**.

Steeneveld, G., M. Wokke, C. Groot Zwaaftink, S. Pijlman, B. Heusinkveld, A. Jacobs, and A. Holtslag, 2010: Observations of the radiation divergence in the surface layer and its implication for its parameterization in numerical weather prediction models. *Journal of Geophysical Research: Atmospheres (1984–2012)*, **115 (D6)**.

Steeneveld, G.-J., 2014: Current challenges in understanding and forecasting stable boundary layers over land and ice. *Frontier is Environmental Science*, **2**, 41.

Steeneveld, G.-J., C. J. Nappo, and A. A. Holtslag, 2009: Estimation of orographically induced wave drag in the stable boundary layer during the cases-99 experimental campaign. *Acta Geophysica*, **57 (4)**, 857–881.

Stensrud, D. J., 2007: *Parameterization schemes: keys to understanding numerical weather prediction models*. Cambridge University Press, New York, USA, 480 pp.

Stull, R. B., 1988: *An introduction to boundary layer meteorology*, Vol. 13. Springer.

Sukoriansky, S., B. Galperin, and V. Perov, 2005: Application of a new spectral theory of stably stratified turbulence to the atmospheric boundary layer over sea ice. *Boundary-Layer Meteorology*, **117 (2)**, 231–257.

Sun, J., L. Mahrt, R. M. Banta, and Y. L. Pichugina, 2012: Turbulence regimes and turbulence intermittency in the stable boundary layer during cases-99. *Journal of the Atmospheric Sciences*, **69 (1)**, 338–351.

Svensson, G., et al., 2011: Evaluation of the diurnal cycle in the atmospheric boundary layer over land as represented by a variety of single-column models: The second gabls experiment. *Boundary-Layer Meteorology*, **140 (2)**, 177–206.

Tastula, 2014: The importance of surface layer parameterization in modeling of stable atmospheric boundary layers. *Atmospheric Science Letters*, in press.

Taylor, K. E., 2001: Summarizing multiple aspects of model performance in a single diagram. *Journal of Geophysical Research: Atmospheres (1984–2012)*, **106 (D7)**, 7183–7192.

Tewari, M., et al., 2004: Implementation and verification of the unified noah land surface model in the wrf model. *20th conference on weather analysis and forecasting/16th conference on numerical weather prediction*, 11–15.

Trier, S., M. LeMone, F. Chen, and K. Manning, 2011: Effects of surface heat and moisture exchange on ARW-WRF warm-season precipitation forecasts over the central united states. *Weather and Forecasting*, **26 (1)**, 3–25.

Van de Wiel, B., A. Moene, H. Jonker, P. Baas, S. Basu, J. Donda, J. Sun, and A. Holtslag, 2012: The minimum wind speed for sustainable turbulence in the nocturnal boundary layer. *Journal of the Atmospheric Sciences*, **69 (11)**, 3116–3127.

Van Heerwaarden, C. C., J. Vilà-Guerau de Arellano, A. F. Moene, and A. A. Holtslag, 2009: Interactions between dry-air entrainment, surface evaporation and convective boundary-layer development. *Quarterly Journal of the Royal Meteorological Society*, **135 (642)**, 1277–1291.

Viterbo, P., A. Beljaars, J.-F. Mahfouf, and J. Teixeira, 1999: The representation of soil moisture freezing and its impact on the stable boundary layer. *Quarterly Journal of the Royal Meteorological Society*, **125 (559)**, 2401–2426.

Vosper, S., E. Carter, H. Lean, A. Lock, P. Clark, and S. Webster, 2013: High resolution modelling of valley cold pools. *Atmospheric Science Letters*, **14 (3)**, 193–199.

Whiteman, C. D., 2000: *Mountain meteorology: fundamentals and applications*. Oxford University Press, New York, USA, 376 pp.

Whiteman, C. D. and J. C. Doran, 1993: The relationship between overlying synoptic-scale flows and winds within a valley. *Journal of Applied Meteorology*, **32 (11)**, 1669–1682.

Wrathall, J., 1985: The mistral and forest fires in provencecôte d'azur, southern france. *Weather*, **40 (4)**, 119–124.

Yang, K., et al., 2008: Turbulent flux transfer over bare-soil surfaces: characteristics and parameterization. *Journal of Applied Meteorology and Climatology*, **47 (1)**, 276–290.

Zannetti, P., 1990: *Air pollution modeling: theories, computational methods, and available software.* Computational Mechanics Southampton.

Zeng, X., Z. Wang, and A. Wang, 2012: Surface skin temperature and the interplay between sensible and ground heat fluxes over arid regions. *Journal of Hydrometeorology*, **13 (4)**, 1359–1370.

887 Zilitinkevich, S., 1995: Non-local turbulent transport: Pollution dispersion aspects of coherent structure

888   of convective flows. *Air Pollution III*, **1**, 53–60.
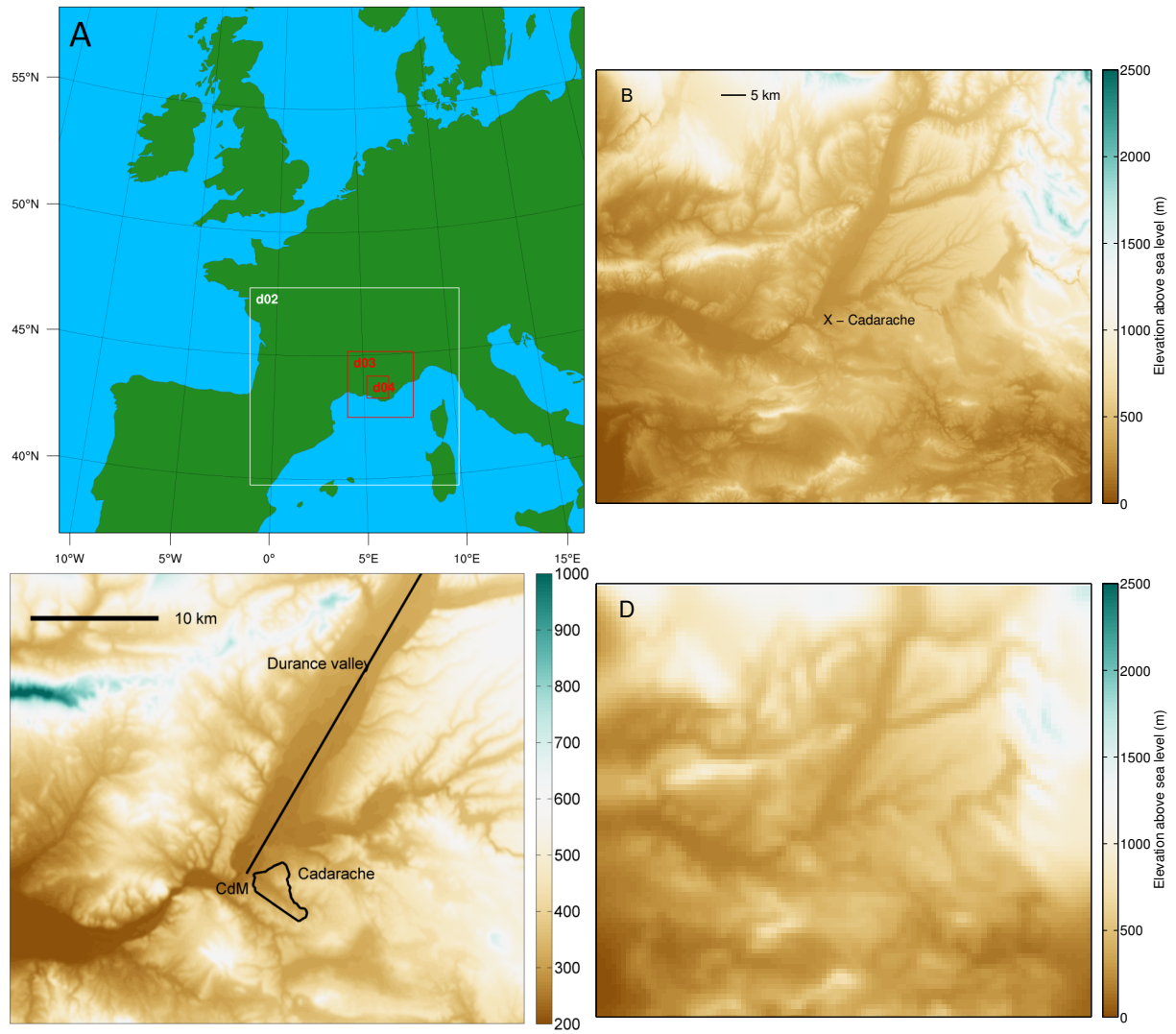
List of Figures

Figure 1: A: WPS domain configuration. The bounds of the outer domain coincide with the border of the figure. B: Orography of domain 4 on high resolution (90 m). C: Zoom of the study area. Durance valley and Cadarache are indicated, as well as the Clue de Mirabeau (CdM). D: Orography of domain 4 as seen by WRF (resolution 1 km).
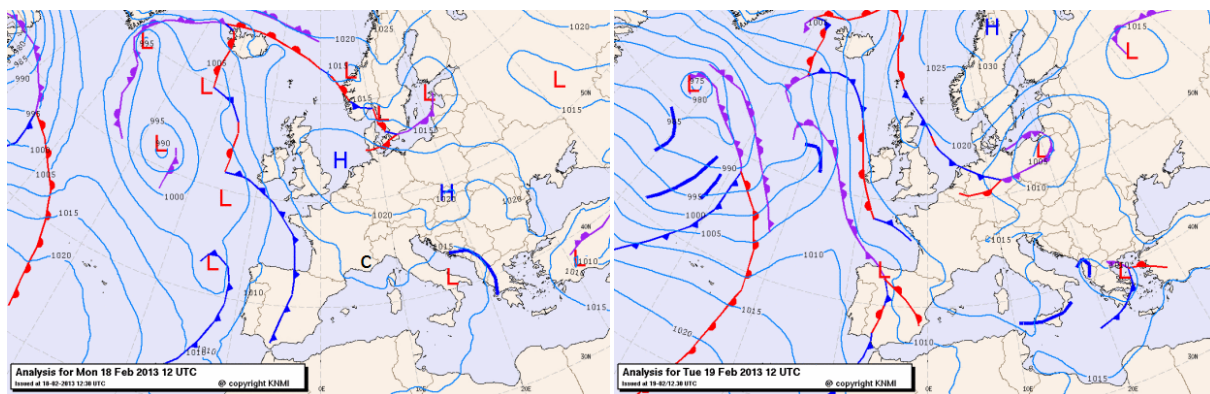
Figure 2: Operational analysis at the start and halfway the simulation. Cadarache is indicated with a 'C'. Source: KNMI.
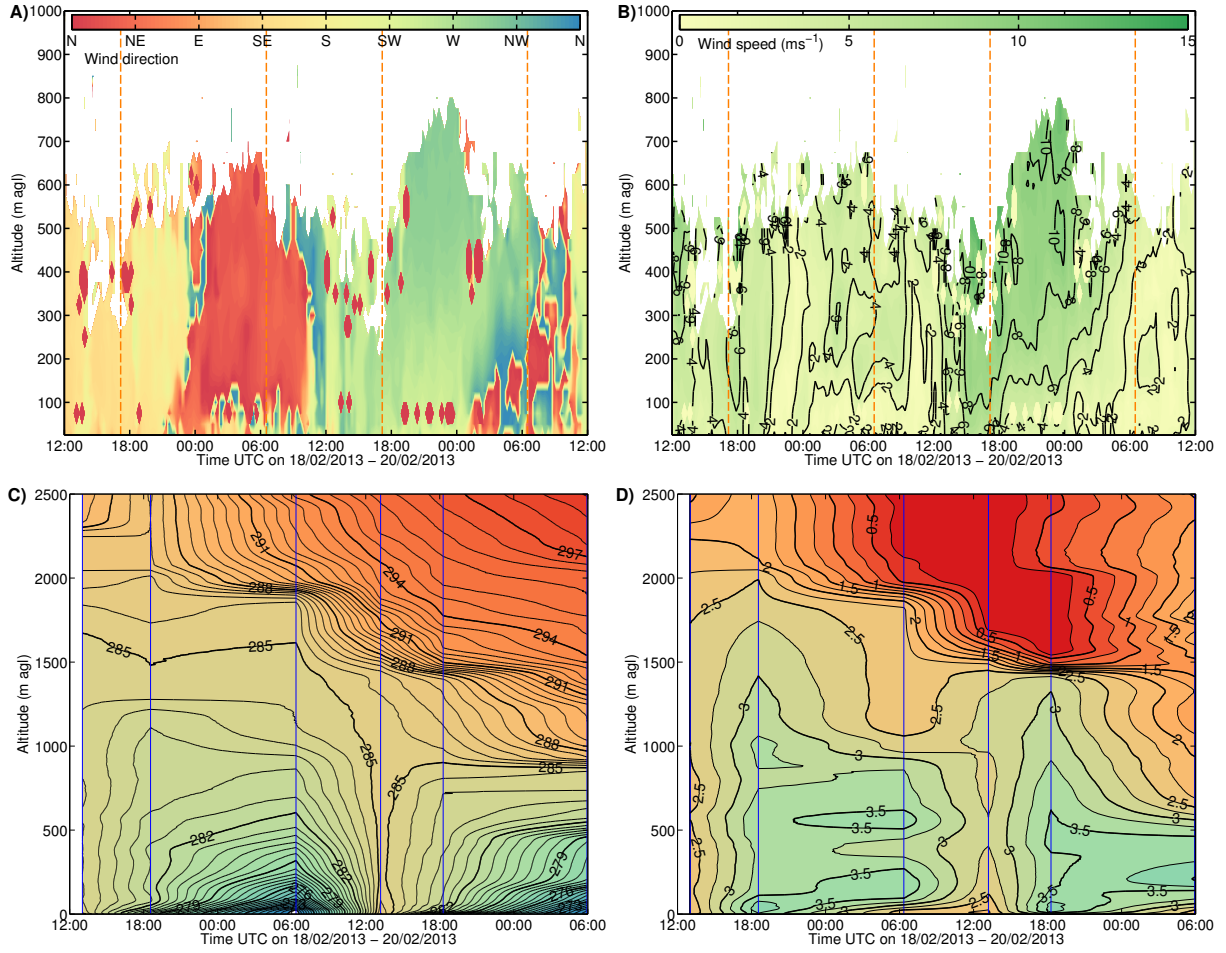
Figure 3: Observed evolution of A) wind direction and B) wind speed, measured by the SODAR, and C) potential temperature (K) and D) mixing ratio (gkg^{-1}) during IOP15 and IOP16. The vertical lines in the lower two plots indicate radiosoundings between which the variables are interpolated. Note that sounding data after 06:00 UTC the on 20th is lacking! In A) and B), the orange vertical lines represent the times of sunset and sunrise.
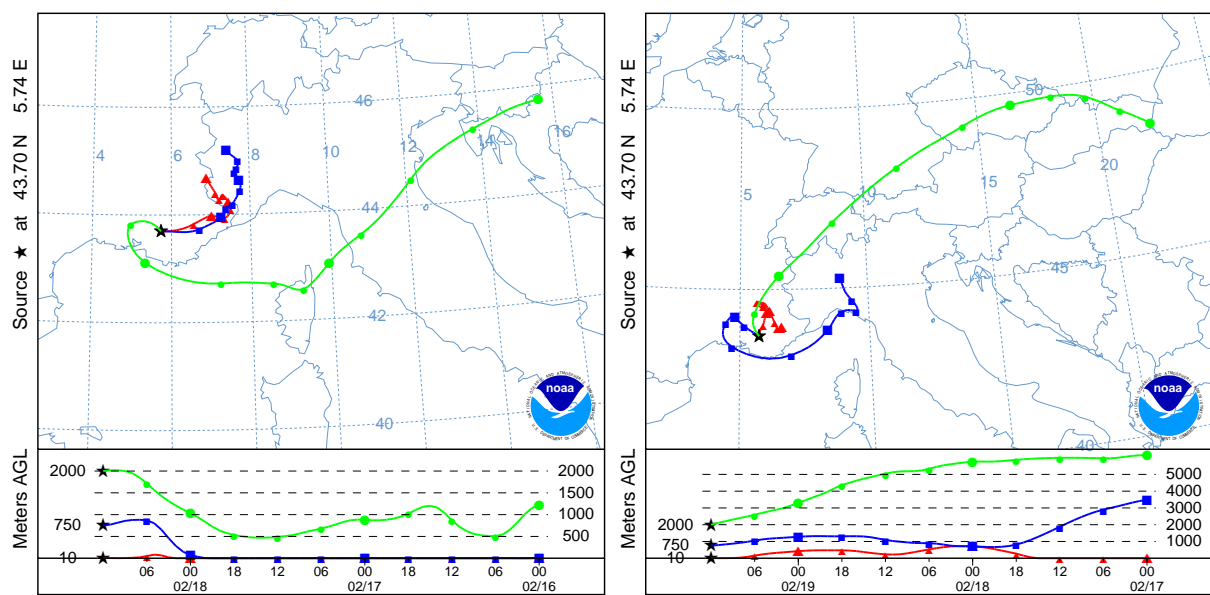
Figure 4: HYSPLIT backward trajectory analysis indicating the source locations of the advected air at three altitudes over Cadarache. Left: 18 February, 12:00 UTC; right: 19 February 12:00 UTC. Source: NOAA Air Resources Laboratory, used with GDAS1 Archive data.
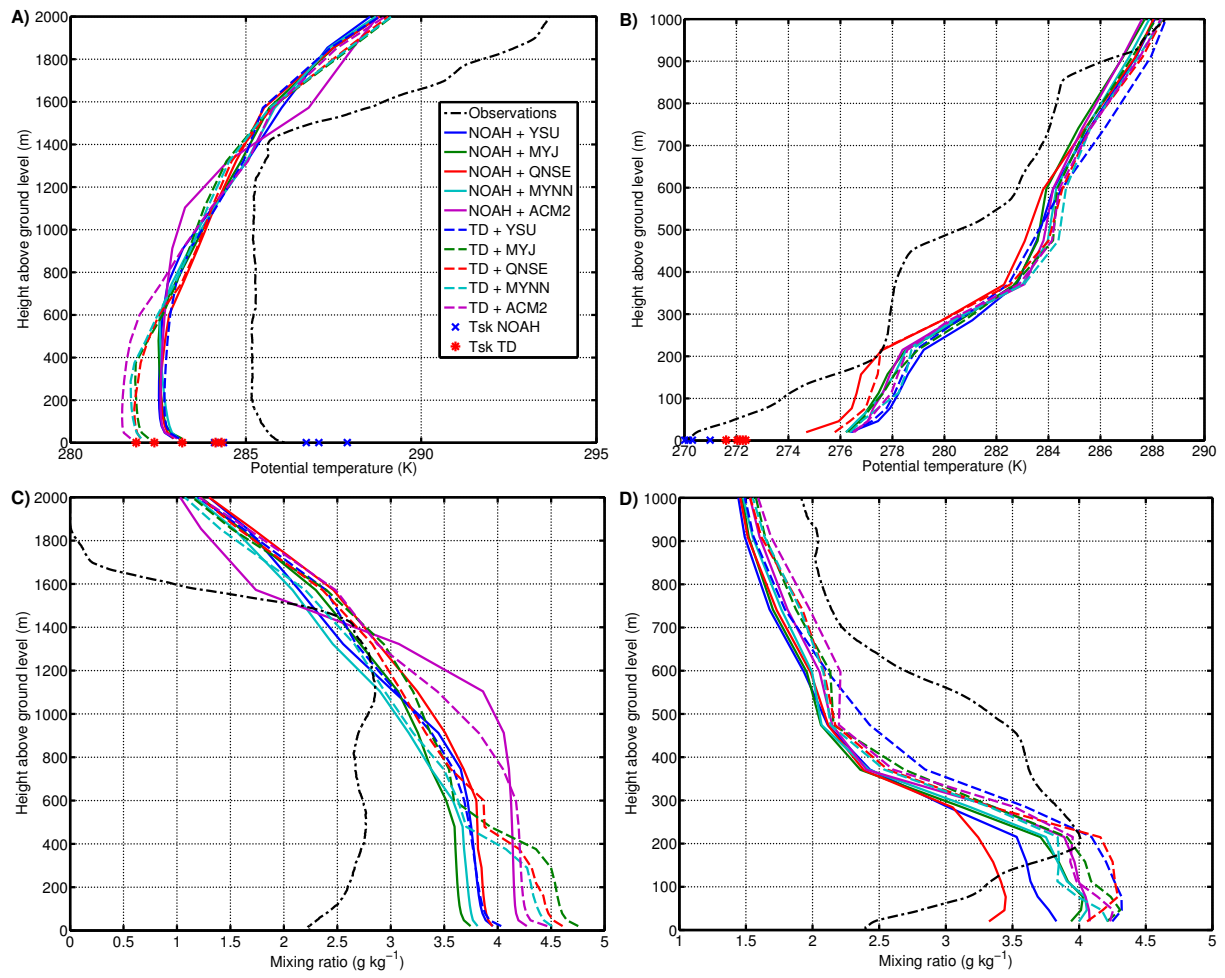
Figure 5: Measured and modelled profiles of A) potential temperature at 12:00 UTC on 19 Feb and B) at 06:00 UTC on 20 February, and mixing ratio at the same times (C and D, respectively) Modelled skin temperature is indicated in A) and B). Note that the axes are different at 12:00 and 06:00!
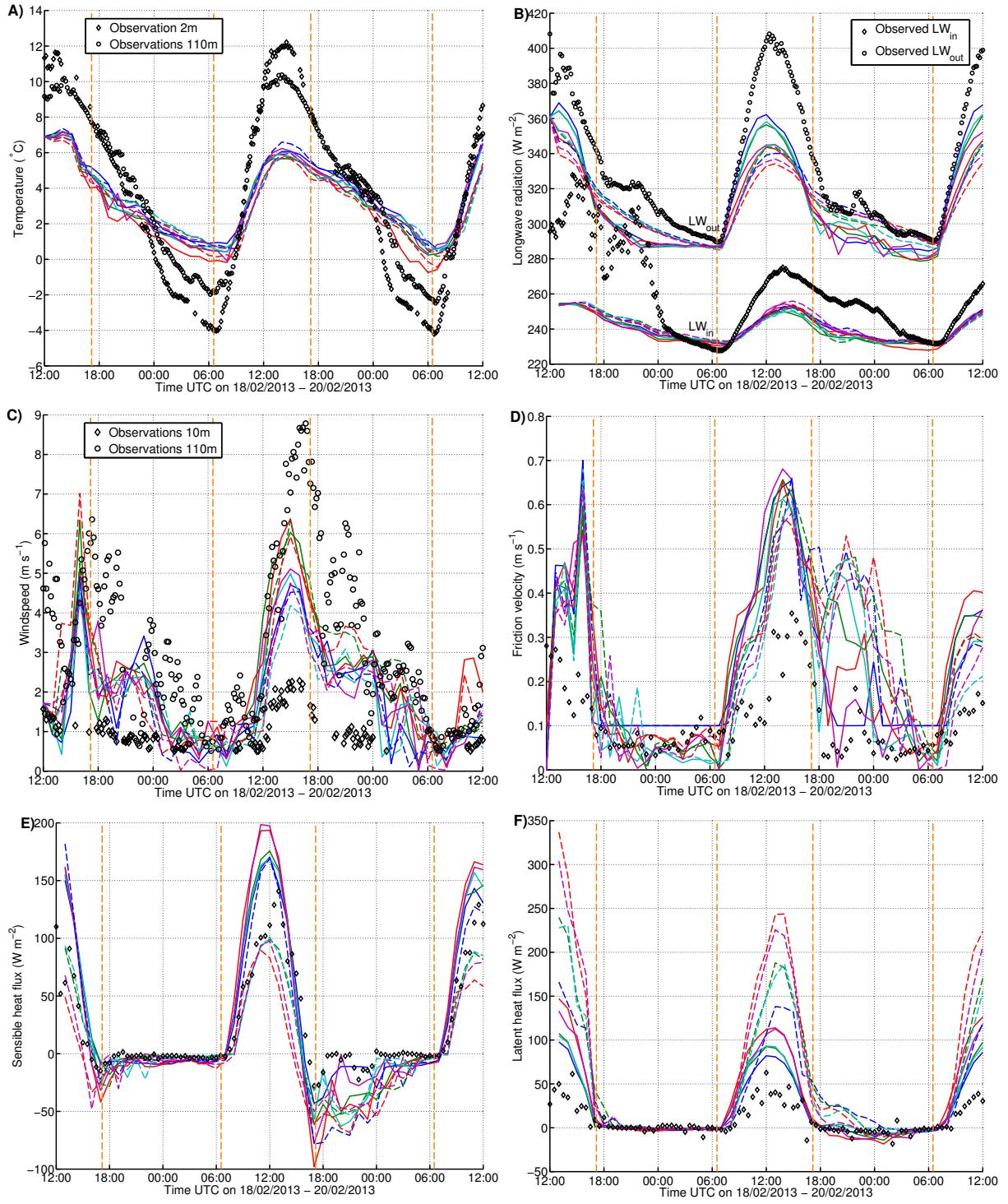
Figure 6: Modelled and measured evolution of A) 110 m temperature, B) longwave radiation components, C) 10 m wind, D) friction velocity, E) sensible heat flux and F) latent heat flux. Legend as in figure 5.
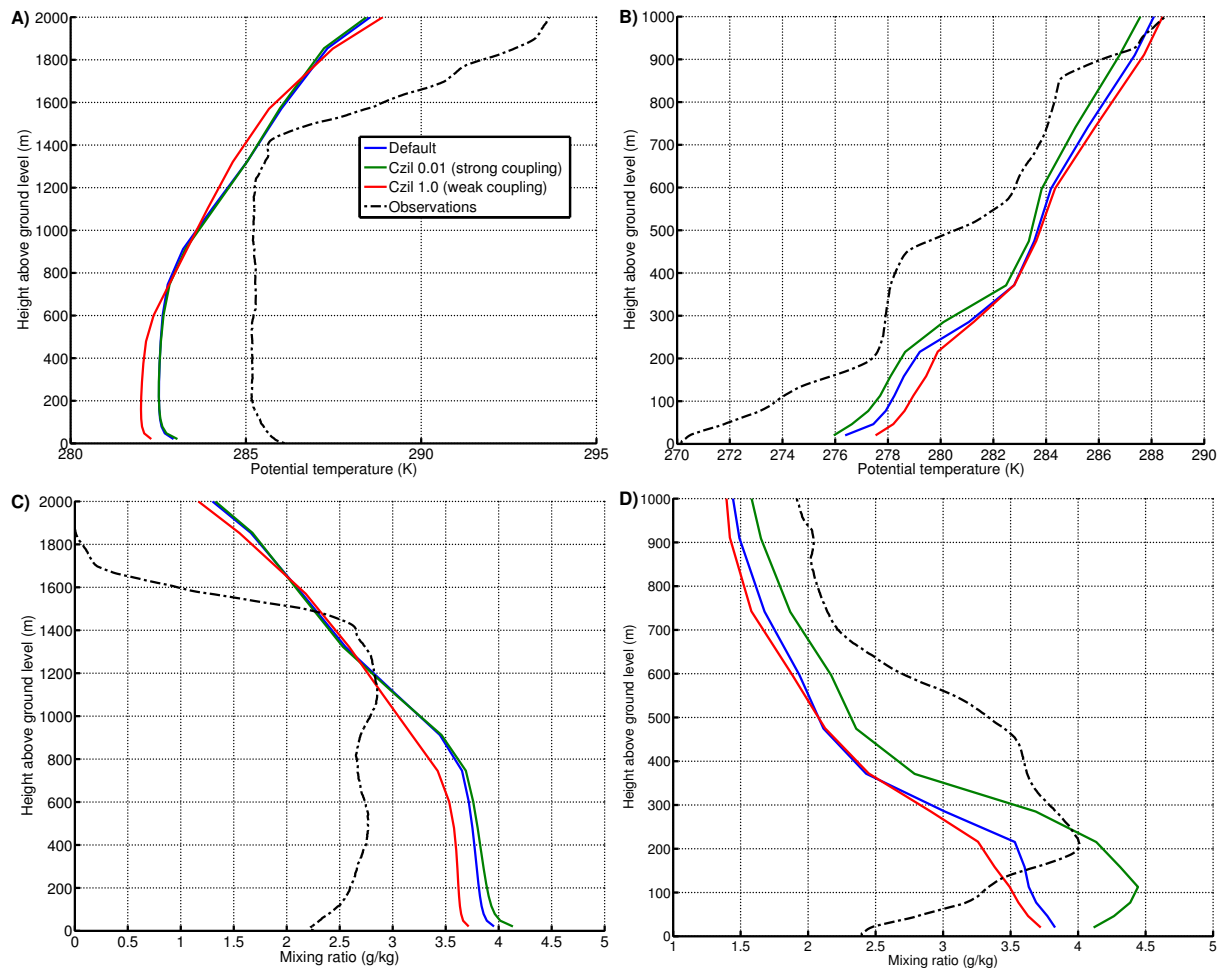
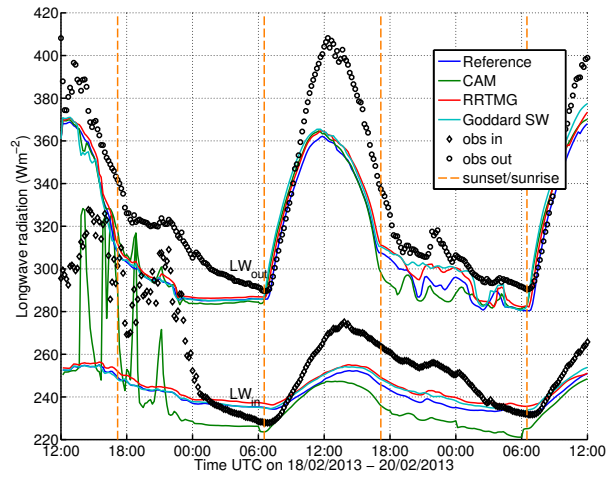Figure 7: Same as figure 5 for strong and weak surface coupling

Figure 8: Modelled (three radiations schemes) and observed longwave radiation components. Reference represents the default run with altered surface layer parameterization (section 4.2.1).
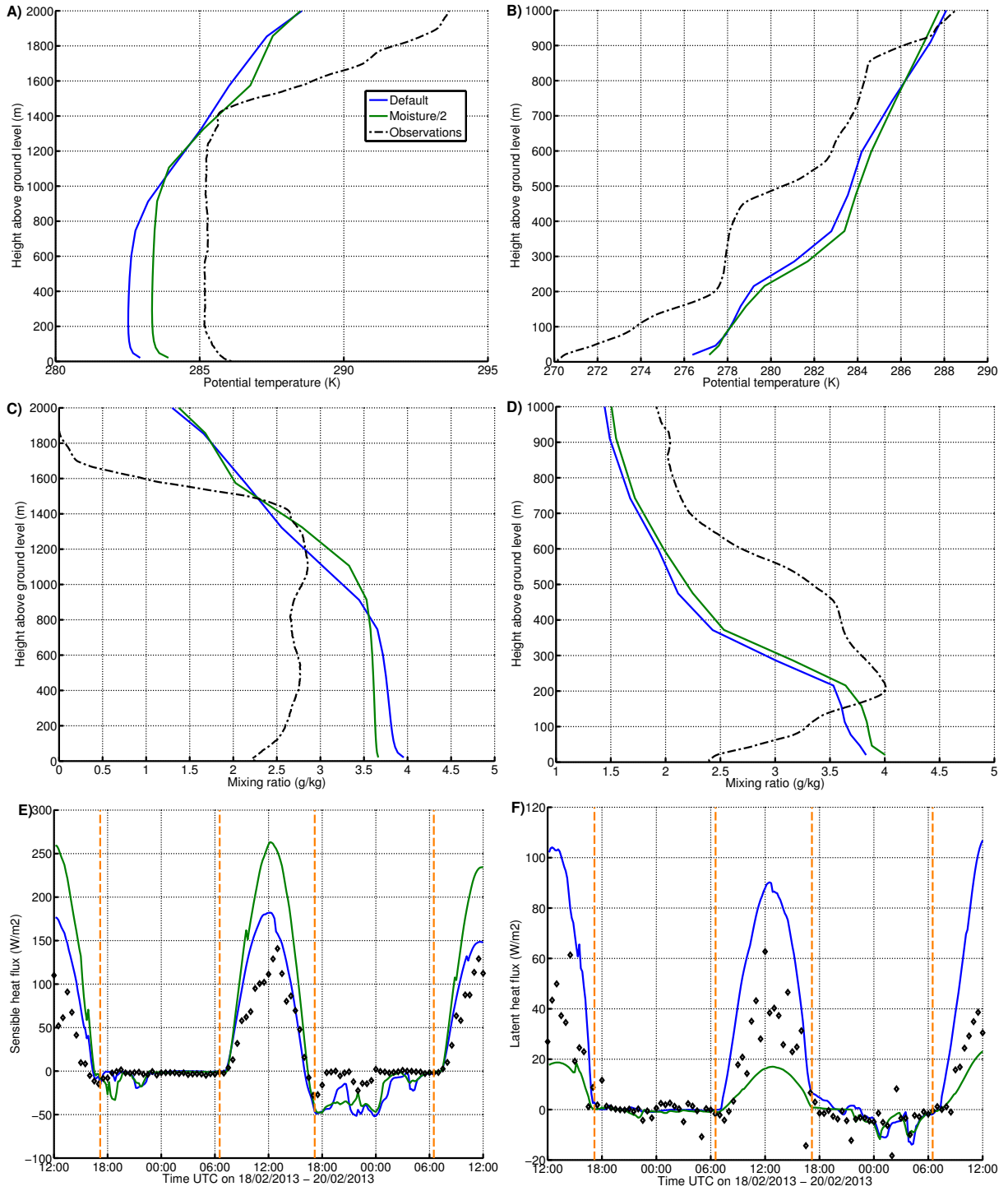
Figure 9: A-D same as figure 5, E and F like figure 6E-F, for reduced soil moisture. Reference is default run but with revised surface layer scheme and RRTMG radiation.
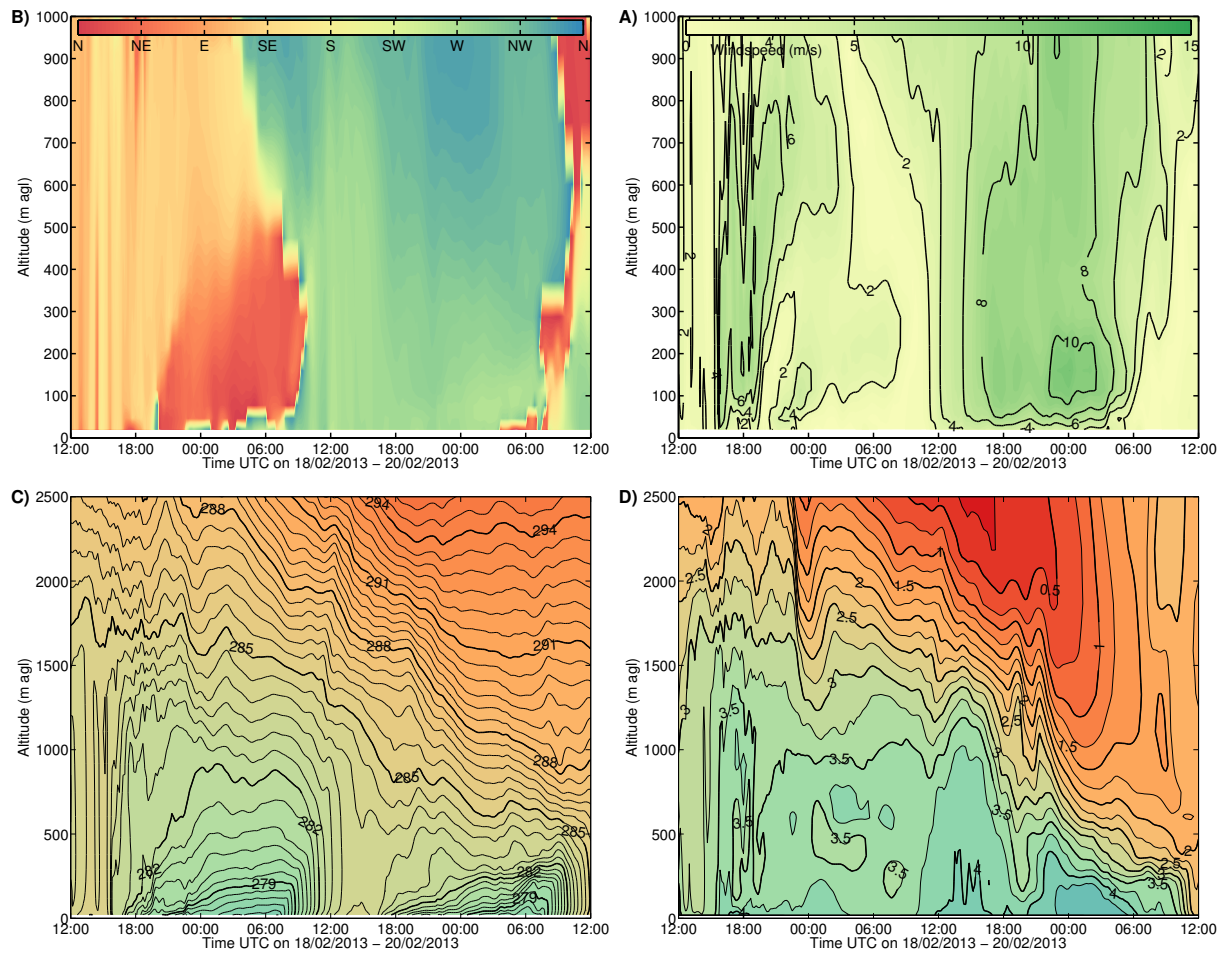
Figure 10: Same as figure 3, for model output from run with revised surface layer scheme and RRTMG radiation. Note that in C) and D), the time axes is extended untill 12:00 UTC.

List of Tables

Table 1: Default settings for all model runs

Model version	WRF 3.5.1
Start date	2013/02/18 12:00 UTC
End date	2013/02/20 12:00 UTC
Spin-up	24 hours
Time step	120 seconds
Domains configuration	4 domains (figure 1)
Parent-child ratio	1 : 3
Nesting	Two-way nested
Grid size inner domain	1 x 1 km
Vertical (eta) levels	35 levels
Land use cover	Corine (2006)
Global data input	ECMWF analysis 0.25°
Microphysics	WSM 6-class (Hong and Lim, 2006)
Longwave radiation	RRTM (Mlawer et al., 1997)
Shortwave radiation	Dudhia (Dudhia, 1989)
Cumulus scheme	Kain-Fritsch (D01 only) (Kain, 2004)
Land surface	**Varied**
Boundary layer	**Varied**

Table 2: Overview of performed model simulations

Run #	Surface scheme	Boundary layer
Run 1	NOAH	YSU
Run 2	NOAH	MYJ
Run 3	NOAH	QNSE
Run 4	NOAH	MYNN2.5
Run 5	NOAH	ACM2
Run 6	TD	YSU
Run 7	TD	MYJ
Run 8	TD	QNSE
Run 9	TD	MYNN2.5
Run 10	TD	ACM2

Table 3: Results of surface layer parameterization experiments. Normalized variance is variance of simulated variable divided by the variance of the observations. Bold number indicate best scores.

	Default	Czil 0.01	Czil 1.0	sfclay_rev	Y08
Centered root mean square difference					
T2 ($°$C)	2.48	**2.36**	3.09	2.68	2.64
T110 ($°$C)	2.24	**2.14**	2.56	2.38	2.38
U10 (ms^{-1})	0.94	**0.85**	1.55	0.96	1.07
U110 (ms^{-1})	2.59	**2.25**	2.76	2.72	2.69
LWin (Wm^{-2})	**19.87**	20.01	20.07	20.37	20.44
LWout (Wm^{-2})	12.14	16.48	16.82	**12.09**	12.13
H (Wm^{-2})	26.90	33.87	**19.51**	28.09	30.33
LvE (Wm^{-2})	18.71	39.87	**6.95**	18.61	18.05
u* (ms^{-1})	0.13	**0.12**	0.18	0.15	0.17
Mean overall bias					
T2 ($°$C)	1.30	**1.01**	1.89	1.55	1.64
T110 ($°$C)	-0.50	-0.91	**-0.27**	-0.32	-0.36
U10 (ms^{-1})	1.18	**1.15**	1.64	1.29	1.40
U110 (ms^{-1})	1.45	**1.16**	1.60	1.51	1.49
LWin (Wm^{-2})	-19.35	-20.00	-18.76	-18.47	**-18.29**
LWout (Wm^{-2})	-18.19	-25.56	**-1.06**	-18.66	-17.40
H (Wm^{-2})	7.08	9.58	-12.10	6.80	**3.41**
LvE (Wm^{-2})	10.99	23.99	**0.83**	11.74	12.68
u* (ms^{-1})	0.12	**0.09**	0.18	0.11	0.13
Correlation coefficient [-]					
T2	**0.97**	0.92	0.96	0.96	0.96
T110	**0.96**	0.95	0.94	0.95	0.95
U10	0.68	**0.75**	0.42	0.63	0.55
U110	0.60	0.61	0.57	0.58	0.57
LWin	0.83	0.80	**0.91**	0.82	0.82
LWout	0.95	**0.96**	**0.96**	0.95	0.95
H	**0.95**	0.93	0.93	0.94	0.93
LvE	**0.92**	0.91	**0.92**	**0.92**	**0.92**
u*	**0.77**	0.74	0.42	0.72	0.66
Normalized variance [-]					
T2	**0.56**	0.67	0.44	0.53	0.53
T110	0.48	**0.52**	0.41	0.45	0.45
LWin	0.29	**0.30**	0.24	0.27	0.26
LWout	**0.81**	0.60	1.32	**0.81**	**0.81**